Dynamic Characteristics of Ball Bearing-Coupling-Rotor System with Angular Misalignment Fault

Pengfei Wang
Northeastern University
Hongyang Xu
Northeastern University
Yang Yang
China North Vehicle Research Institute
Hui Ma (mahui_2007@163.com)
Northeastern University
Duo He
Northeastern University
Xiang Zhao
Northeastern University

Research Article

Keywords: Ball bearing-coupling-rotor system, Misalignment fault, Axial vibration, Rotor dynamics, Finite element

Posted Date: December 14th, 2021

DOI: https://doi.org/10.21203/rs.3.rs-1127803/v1

Version of Record: A version of this preprint was published at Nonlinear Dynamics on April 25th, 2022.
See the published version at https://doi.org/10.1007/s11071-022-07451-1.

Dynamic characteristics of ball bearing-coupling-rotor system with angular misalignment fault

Pengfei Wang [a], Hongyang Xu [a], Yang Yang [b], Hui Ma [a,c*], Duo He [a], Xiang Zhao [a]

[a] *School of Mechanical Engineering and Automation, Northeastern University, Shenyang, Liaoning 110819, P R China*

[b] *China North Vehicle Research Institute, Beijing 100072, P R China*

[c] *Key Laboratory of Vibration and Control of Aero-Propulsion System Ministry of Education, Northeastern University, Shenyang, Liaoning 110819, P R China*

Abstract

The rotor misalignment fault, which occurs only second to unbalance, easily occurs in the practical rotating machinery system. Rotor misalignment can be further divided into coupling misalignment and bearing misalignment. However, most of the existing references only analyze the effect of coupling misalignment on the dynamic characteristics of the rotor system, and ignore the change of bearing excitation caused by misalignment. Based on the above limitations, a five degrees of freedom nonlinear restoring force mathematical model is proposed, considering misalignment of bearing rings and clearance of cage pockets. The finite element model of the rotor is established based on the Timoshenko beam element theory. The coupling misalignment excitation force and rotor unbalance force are introduced. Finally, the dynamic model of the ball bearing-coupling-rotor system is established. The radial and axial vibration responses of the system under misalignment fault are analyzed by simulation. The results show that the bearing misalignment significantly influences the dynamic characteristics of the system in the low-speed range, so bearing misalignment should not be ignored in modeling. With the increase of rotating speed, rotor unbalance and coupling misalignment have a greater impact. Misalignment causes periodic changes in bearing contact angle, radial clearance, and ball rotational speed. It also leads to reciprocating impact and collision between the ball and cage. In addition, misalignment increases the critical speed and the axial vibration of the system. The results can provide a basis for health monitoring and misalignment fault diagnosis of the rolling bearing-rotor system.

Keywords: Ball bearing-coupling-rotor system; Misalignment fault; Axial vibration; Rotor dynamics; Finite element

---

* Corresponding author.

E-mail address: mahui_2007@163.com (H. Ma)

List of symbols

A_j	Relative distance between curvature centers of inner and outer raceways after initial misalignment
A_j'	Relative distance between curvature centers of inner and outer raceways after vibration
c_c	Clearance of cage pocket
c_r	Initial radial clearance of rolling bearing
c_{rj}'	Radial clearance at the position of the j-th ball after misalignment
$\boldsymbol{C}_s$	Rotor damping matrix
d_b	Ball diameter
d_m	Bearing pitch diameter
$\boldsymbol{D}_{dp}$	Disc element gyro matrix at the node p
e_{dp}	Disc eccentricity at the node p
f_i, f_o	Curvature radius coefficient of inner and outer raceway
f_r	Rotating frequency
f_{vc}	Varying compliance vibration frequency of rolling bearing
$\boldsymbol{F}_b$	Nonlinear force vector of rolling bearing
F_{bj}	Contact force between the j-th ball and the raceway
F_{bx}, F_{by}, F_{bz}	Nonlinear restoring force component of rolling bearing along X, Y and Z directions
$\boldsymbol{F}_c$	Coupling misalignment force vector
F_{cx}, F_{cy}	Misalignment force component of coupling along X and Y directions
$\boldsymbol{F}_e$	Rotor unbalance force vector
F_{epx}, F_{epy}	Unbalance force component of rotor along X and Y directions
$\boldsymbol{G}$	Rotor gravity vector
h_d	Disc thickness
$\boldsymbol{J}_d$	Disc gyro matrix
J_{dp}, J_{pp}	Diameter /polar moment of inertia of the disk at node p
$\boldsymbol{J}_s$	Gyro matrix of shaft
$\boldsymbol{J}_{sq}$	Gyro matrix of the q-th shaft element
k_{bj}	Hertz contact stiffness between the j-th ball and the raceway
$\boldsymbol{K}_s$	Stiffness matrix of shaft
$\boldsymbol{K}_{sq}$	Stiffness matrix of the q-th shaft element
l	Length of rotor
M_{bx}, M_{by}	Nonlinear restoring torque of rolling bearing around X and Y axes
$\boldsymbol{M}_d$	Disc mass matrix
m_{dp}	Disc mass at node p
$\boldsymbol{M}_{dp}$	Disc mass matrix at node p
$\boldsymbol{M}_s$	Shaft mass matrix
$\boldsymbol{M}_{sq}$	Mass matrix of the q-th shaft element
N_b	Number of bearing balls
r_b	Raceway radius of bearing inner ring
r_d	Inner radius of disc
r_{dj}	Radial distance of curvature center of inner raceway at the j-th ball angle position
r_i, r_o	Curvature radius of inner/outer ring of bearing raceway
R_b	Raceway radius of bearing outer ring
R_d	Outer radius of disc

$\boldsymbol{U}$	Rotor displacement vector
$\boldsymbol{U}_q$	Displacement vector of the q-th shaft element
α_j	Initial contact angle of the j-th ball after misalignment
α_j'	contact angle of the j-th ball after vibration
δ	Misalignment of coupling
δ_j	Contact deformation between the j-th ball and the raceway
θ_{01}	Initial position angle of the first ball
θ_j	Position angle of the j-th ball
φ	Misalignment angle
φ_x, φ_y	Misalignment angle of bearing ring around X and Y axes
ω_{bj}	Revolution angular velocity of the j-th ball
ω_c	Rotating angular velocity of cage
ω_r	Rotating angular velocity of rotor
Δ_j	The normal clearance caused by the angular position of the j-th ball.
Δl	Distance between two coupling halves
$\sum\rho_{in}$, $\sum\rho_{out}$	Sum of curvature of inner/outer raceway of bearing.

1. Introduction

As the core component of modern aero-engine, the rotor system often uses rolling bearing as its supporting element. Misalignment faults often occur in rolling bearing-rotor systems due to improper machining and assembly, load, or temperature changes during operation. According to statistics, misalignment, as a fault form second only to rotor unbalance, can account for 70% of the whole rotor system faults [1]. Rotor misalignment can be divided into coupling misalignment and bearing misalignment according to the fault location. The coupling misalignment can be further subdivided into deflection angle misalignment, parallel misalignment, and combination misalignment. Harris [2] subdivided the misalignment of rolling bearing into out-of-line, tilted outer ring, tilted inner ring, and shaft deflection. If the assembly coaxiality error of the rotor system is large, the misalignment fault of coupling and rolling bearing may coincide. Misalignment of the coupling not only aggravates the system vibration but also causes other faults such as rub impact between rotor and casing, shaft crack, and so on. It has been pointed out clearly in the standard ISO 15243 that the bearing misalignment will also lead to fatigue fracture of bearing cage [3] and finally cause bearing failure, as shown in Fig. 1. In severe cases, the misalignment fault will further lead to engine shutdown and then cause great losses of aircraft destruction and human death. Therefore, it is of significant significance to study the dynamic characteristics of the rolling bearing-rotor system under the combined action of coupling and bearing misalignment for dynamic design, fault detection and diagnosis of the system during installation and operation.

Fig. 1 Fracture failure of rolling bearing cage of aero-engine [4]

The research literature on coupling misalignment and rolling bearing misalignment can be dated back to the 1970s. In the study of rotor-coupling misalignment, the most important thing is to establish a mathematical expression that can simulate coupling misalignment. At present, the main modeling methods of coupling misalignment can be divided into the following three types: (1) According to the geometric relationship and force analysis of misalignment, the expression of excitation force generated by coupling misalignment is obtained [5-10]. (2) Based on the Lagrange energy method, the dynamic equation of misalignment coupling-rotor system is established [11-13]. (3) The coupling is regarded as shaft element or lumped mass point, and it is grouped with the finite element model (FEM) of rotor [14-18]. Gibbons [5] established the coordinate system of coupling parallel misalignment, and then proposed the calculation formulas of additional force and torque under the action of parallel misalignment. Subsequently, Sekhar and Prabhu [6] further gave the excitation force expression of coupling angular misalignment on this basis. Lee and Lee [7] gave the decomposition formula of coupling misalignment force, and combined with the nonlinear rolling bearing force model of five degrees of freedom (5-DOF). The nonlinear vibration characteristics of the rolling bearing-rotor system under coupling misalignment fault were discussed by experiment and simulation. In addition, Zhao et al. [8] proposed a meshing force model of spline coupling under misalignment fault, and numerically simulated and analyzed the influence law of spline coupling misalignment on the dynamic characteristics of the rotor system. Wu et al. [9] proposed the equation for calculating the excitation force of elastic coupling under dynamic spatial misalignment (DSM), and analyzed the vibration response of rotor system with DSM and unbalance. Al-Hussain [11] established a symmetrical double-span Jeffcott rotor with angular misalignment fault through Lagrange energy equation, and analyzed the internal relationship between the misalignment degree of coupling and the stable operation of the system. Patel and Darpe [14] proposed a method to determine the magnitude of misalignment excitation and harmonic excitation based on experiments, established the FEM of a coupled rotor with the Timoshenko beam element, and simulated the coupling misalignment effect of rotor by node force vector. Then, they studied the steady-state

response of the rotor at subcritical speed, and compared the difference between parallel misalignment and angular misalignment in the bending-axial-torsional coupling vibration characteristics of the rotor system.

In terms of the research on the influence of coupling misalignment fault on the dynamic characteristics of the rotor system, Bouaziz et al. [19] studied the dynamic characteristics of misalignment rotor system supported by active magnetic bearing numerically. They found that the frequency spectrum of angular misalignment fault is mainly 2 times of rotating frequency ($2f_r$) and 4 times of rotating frequency ($4f_r$). Patel and Darpe [20] carried out an experimental study on the misalignment problem of the rotor-coupling system. It was found that the axis trajectory showed outer looped orbits under the angular misalignment fault, while the axis trajectory showed inner looped orbits under the parallel misalignment fault. The full spectrum is better than the FFT Spectrum for coupling misalignment fault diagnosis. Lu et al. [21] built a simple aero-engine dual-rotor test-bed, established the FEM of the test-bed system, introduced the nonlinear force of rolling bearing and coupling misalignment fault, reduced the dimension of the system by the proper orthogonal decomposition method, and discussed the spectral characteristics of misalignment fault of the dual-rotor-bearing system. In fact, once the misalignment fault occurs, other coupling faults may further occur in the rotor system, and the most common is the unbalance and misalignment coupling faults [22-24]. In addition, rubbing and misalignment coupling faults [25,26], loosening and misalignment coupling faults [27], fluid excitation of sliding bearing and misalignment coupling faults [25,28,29] may also occur. For example, taking the turbine generator rotor system as the research object, Fu et al. [25] established the nonlinear dynamic model of rubbing-unbalance-misalignment coupling fault under the action of nonlinear oil-film force, and verified by experiment. The results showed that the system moves periodically at low speed, and the vibration energy is mainly the frequency of f_r and $2f_r$. However, with the increase of rotating speed, the vibration energy of the system is gradually dominated by subharmonic frequency components under the action of oil film force and rubbing force. Jin et al. [26] further analyzed the nonlinear vibration characteristics of blade-casing rubbing caused by misalignment of the aero-engine dual-rotor-rolling bearing system. Ma et al. [28] simulated and studied the oil film instability law of the cantilever rotor system with parallel and angular misalignment during speed up and down, and found that the coupling misalignment delays the occurrence of first-order oil-film instability.

In terms of the research on the misalignment of rolling bearing, Hinton's literature [30] showed that in the late 1940s, the Royal Air Force had many cases of cage fracture caused by misalignment of bearing assembly, which led to the failure of ball bearing in aero-engine. Crawford [31] found through experimental tests that when the misalignment angle of rolling bearing increased from 0.26° to 0.61°, the dynamic stress of the cage soared from 0.172 MPa to 3.45 MPa, which increased by about 2006%. This further indicated that abnormal cage stress

caused by bearing misalignment is the main cause of cage fatigue fracture. Xu et al. [32] analyzed the failure of the ground bench test of an aero-engine, and found that the first broken part of bearing was the cage, and the bearing tilt after engine assembly was the main cause of bearing failure. Ertas and Vance [33] built a liquid hydrogen fuel turbopump test-bed. The test found that static misalignment will increase the radial stiffness of angular contact ball bearing, while dynamic misalignment would reduce the radial stiffness of bearing. At present, the modeling methods of bearing misalignment can be mainly divided into stiffness model calculated by static and quasi-static methods [34-42], and nonlinear force model [43, 44]. Zhang et al. [35] derived an improved quasi-static angular contact ball bearing model, discussed the influence of misalignment on bearing load distribution, stiffness and life under axial load and combined load. The influence of two kinds of bearing misalignment on the natural frequency of the bearing-rotor system was compared and analyzed. At present, many references give the misalignment value directly. But in fact, the value of bearing misalignment is uncertain. Yang et al. [37] studied the influence of angular contact ball bearing on raceway wear in spindle system under initial uncertain misalignment, and found that the wear depth of inner raceway is significantly greater than that of the outer raceway. Yi et al. [43] took the machine tool spindle-angular contact ball bearing as the research object. A relatively simple 2-DOF nonlinear force model of rolling bearing with parallel misalignment was proposed. The research found that bearing misalignment significantly impacts the dynamic characteristics and amplitude of the system. Taking double-row angular contact ball bearing as the research object, Parmar et al. [44] considered the influence of bearing outer ring defects and bearing angular misalignment, and proposed the expression of a 3-DOF nonlinear restoring force model considering bearing angular misalignment. The vibration response of bearing was studied, and relevant experimental research was carried out.

From the current research situation, the research on the dynamics and vibration of the misaligned rotor system mainly focuses on coupling misalignment. Many scholars have carried out a lot of theoretical and experimental researches in this field, and achieved fruitful research results. However, there is relatively little research on the misalignment of rolling bearing. The existing reference mainly focuses on the impact of bearing misalignment on its static performance, such as the stiffness, contact problem and fatigue life of bearing itself. However, there is relatively little research on its dynamic performance, especially in the impact of bearing misalignment on the dynamic characteristics of the rotor system. Besides, because the interference fit is generally adopted between the rolling bearing and the rotating shaft, once the coaxiality error of the rotor assembly is too large, the rotating shaft tilt may also cause a certain tilt of the bearing inner ring relative to the outer ring, and then induce the bearing misalignment fault. However, in the dynamic response study of misalignment fault of ball bearing-coupling-rotor system, only misalignment excitation of coupling is considered, and the change of bearing

excitation caused by misalignment is ignored. There are few reports on the dynamic characteristics of rolling bearing and coupling misalignment.

Based on the limitations of existing research, this paper firstly deduces a 5-DOF nonlinear bearing force model based on the Hertz contact theory, which can take angular misalignment into account. At the same time, the model also includes uneven ball distribution caused by the cage pocket clearance. Secondly, the finite element dynamic model of the rotor system is constructed based on the Timoshenko beam element theory. The coupling misalignment force and the rolling bearing misalignment force are introduced into the rotor dynamic model. Finally, the radial and axial vibration responses of the rotor system under the combined action of angular misalignment of coupling and rolling bearing are analyzed. The research results can provide theoretical support for dynamic monitoring and fault diagnosis of misalignment fault in the rolling bearing-rotor system.

2. Dynamic model of ball bearing-coupling-rotor system with angular misalignment

In the actual aero-engine rotor system, since the mass is mainly concentrated in the compressor and turbine, the low-pressure rotor of the aero-engine is simplified into a single-span double-disc rotor system supported by rolling bearings. The structural diagram is shown in Fig. 2(a). Due to improper installation and other reasons, the coaxiality error between the rear support bearing seat and the rotor center is large, and there is a height difference Δ between the two ends of the bearing seat. If the bending deformation of the rotor is ignored, the misalignment angle φ can be approximated by the relation between the length of the rotor l and the height difference Δ. Besides, the interference fit is generally used for bearing inner ring and the rotating shaft, so in this case, the system should have two fault forms: angle misalignment of coupling and inner ring tilt misalignment of bearing. Given that the total length of the rotor is 597 mm, it is divided into 27 shaft segments by the finite element method, and each shaft segment is simulated by the Timoshenko beam element, as shown in Fig. 2(b). There are two discs at the front and rear of the rotor, which are arranged asymmetrically. The diameter of each disc is 190 mm, and the thickness is 10 mm. The disc is simplified as a lumped mass point, as shown in Fig. 2(c), and it is placed at nodes 11 and 18 of the rotor, respectively. Both the rotor ends are supported by the 6205 deep groove ball bearings at nodes 7 and 24 of the rotor.

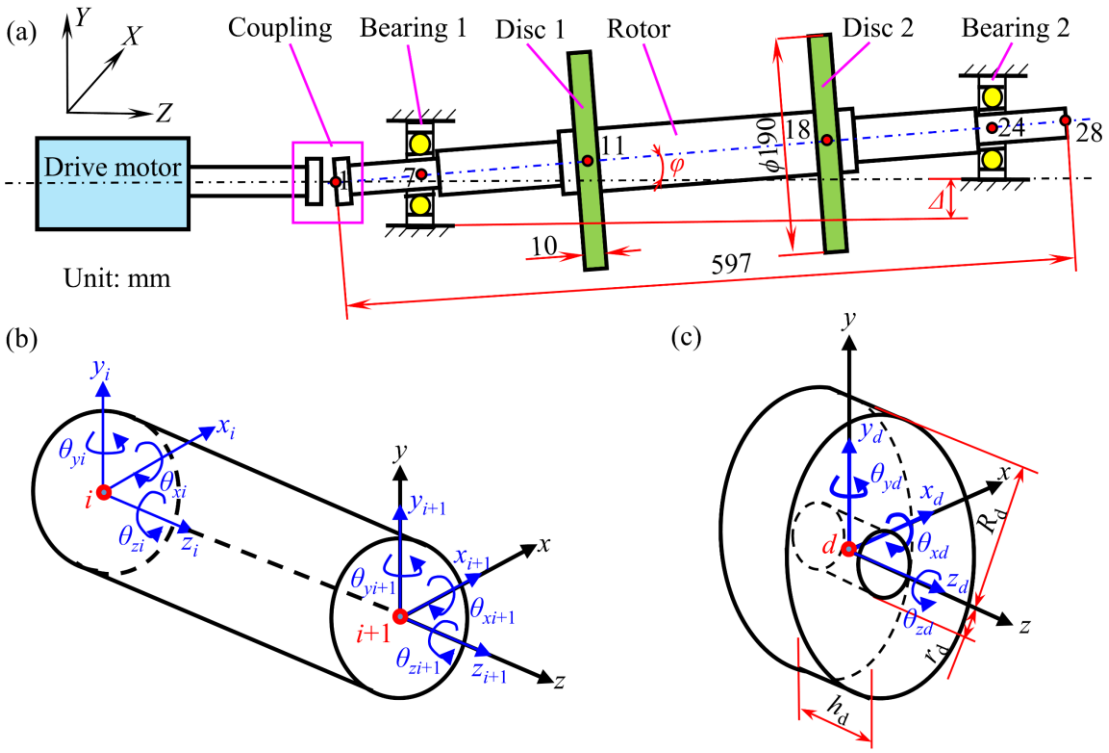

Fig. 2 (a) Schematic of bearing-rotor system, (b) schematic of shaft segment element, (c) schematic of disc element

2.1. Misalignment model of bearing

The schematic of the deep groove ball bearing is shown in Fig. 3. It is assumed that the number of bearing balls is N_b. The inner and outer raceway radii are r_b and R_b, respectively. The ball diameter is d_b. The bearing pitch diameter is d_m, and its size is the sum of the inner and outer raceway radii. The initial radial clearance of the bearing is c_r, and the clearance of the cage pocket is c_c. For the convenience of research, the following assumptions are made: (1) The ball in the bearing makes pure rolling between the inner and outer raceways. (2) The effects of lubricating oil, temperature and ball centrifugal force are not considered.

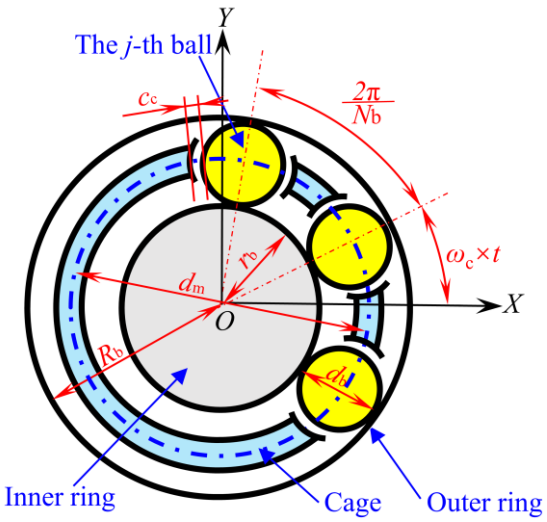

Fig.3 Schematic of deep groove ball bearing

Without loss of generality, this paper first assumes that there is an initial misalignment in the installation process of the rotating shaft, which leads to the bearing inner ring tilting along the X-axis at an angle of φ_x, as shown in Fig. 4(a). The geometric relationship after misalignment of the bearing inner ring is shown in Fig. 4 (b). Where, the angular position of the j-th ball is θ_j, and the central position point of the ball is O_{bj}. The contact point between the j-th ball and the curvature center of the outer raceway is O_{oj}, and the contact point with the curvature center of the inner raceway is O_{ij}. The curvature center trajectory of the inner raceway also changes when the inner raceway tilt is misaligned. The contact point between the j-th ball and the inner raceway becomes O_{ij}', and the center point of the ball becomes O_{bj}'.

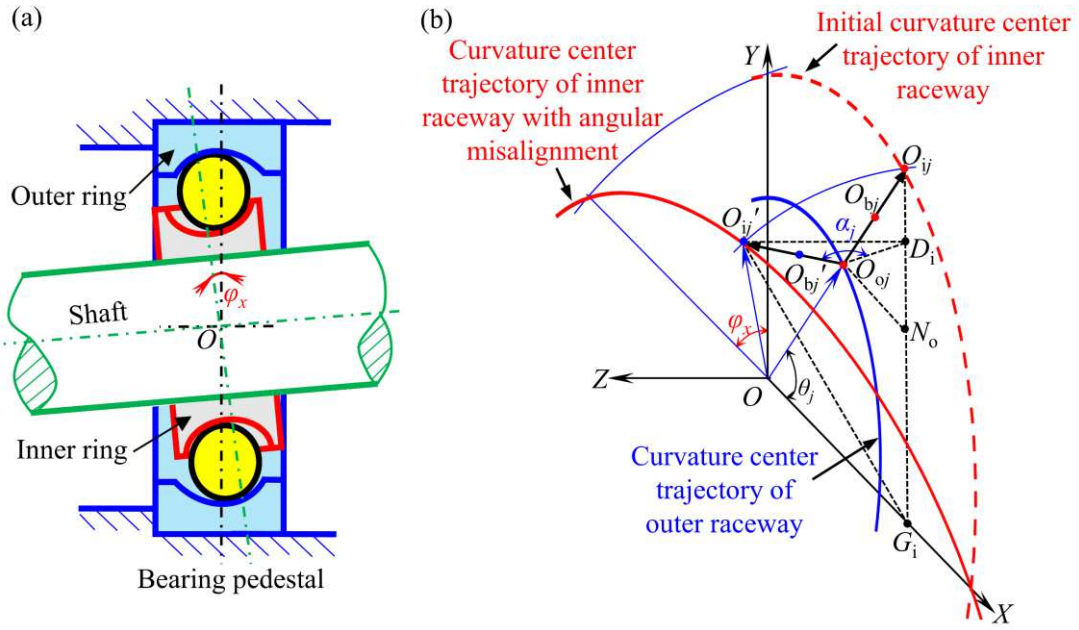

Fig.4 Schematic of bearing inner ring misalignment

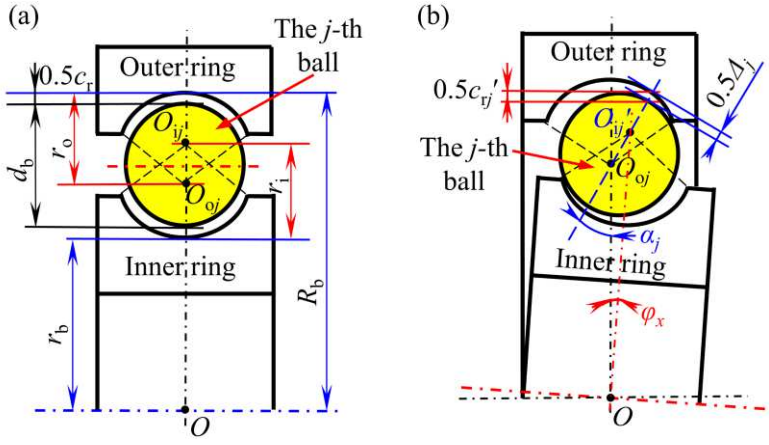

Fig.5 Schematic of bearing geometric relationship

In Fig. 4 (b), the radius of curvature center of the inner and outer raceway is $\left|\overrightarrow{OO_{ij}}\right|$ and $\left|\overrightarrow{OO_{oj}}\right|$ respectively. Combined with the geometric relationship shown in Fig. 5 (a), they can be expressed as:

$$\left|\overrightarrow{OO_{ij}}\right| = r_b + r_i, \quad \left|\overrightarrow{OO_{oj}}\right| = R_b - r_o \tag{1}$$

In Eq. (1), r_i and r_o are curvature radii of inner and outer raceways respectively, and the curvature radius coefficient $f_{i/o}$ of the inner/outer raceway is introduced. Therefore, the curvature radius of inner/outer raceway of the bearing can be expressed as the product of their curvature radius coefficient and ball diameter:

$$r_i = f_i d_b, \qquad r_o = f_o d_b \tag{2}$$

Therefore, the geometric relationship can be obtained according to Fig. 4 (b) as follows:

$$\left|\overrightarrow{D_i O_{ij}'}\right| = \left(r_b + r_i\right)\sin\theta_j \sin\varphi_x \tag{3}$$

$$\left|\overrightarrow{D_i O_{ij}}\right| = \left|\overrightarrow{G_i O_{ij}}\right| - \left|\overrightarrow{G_i D_i}\right| = (r_b + r_i)\sin\theta_j (1-\cos\varphi_x) \tag{4}$$

$$\left|\overrightarrow{O_{oj} N_o}\right| = \left|\overrightarrow{O_{oj} O_{ij}}\right|\cos\theta_j = (r_i + r_o - d_b - c_r)\cos\theta_j \tag{5}$$

$$\left|\overrightarrow{N_o D_i}\right| = \left|\overrightarrow{N_o O_{ij}}\right| - \left|\overrightarrow{D_i O_{ij}}\right| = [(r_i + r_o - d_b - c_r) - (r_b + r_i)(1-\cos\varphi_x)]\sin\theta_j \tag{6}$$

$$\begin{aligned}\left|\overrightarrow{O_{oj} D_i}\right| &= \sqrt{\left(\left|\overrightarrow{O_{oj} N_o}\right|\right)^2 + \left(\left|\overrightarrow{N_o D_i}\right|\right)^2} \\ &= \sqrt{\left(r_i + r_o - d_b - c_r\right)^2 \cos^2\theta_j + [(r_i + r_o - d_b - c_r) - (r_b + r_i)(1-\cos\varphi_x)]^2 \sin^2\theta_j}\end{aligned} \tag{7}$$

According to Fig. 4(b) and Fig. 5(b), the contact angle α_j and normal clearance Δ_j generated at the angular position of the j-th ball due to bearing misalignment can be expressed as:

$$\alpha_j = \arctan\left(\frac{\left|\overrightarrow{D_i O_{ij}'}\right|}{\left|\overrightarrow{O_{oj} D_i}\right|}\right) \tag{8}$$

$$\Delta_j = r_i + r_o - d_b - \sqrt{\left(\left|\overrightarrow{D_i O_{ij}'}\right|\right)^2 + \left(\left|\overrightarrow{O_{oj} D_i}\right|\right)^2} \tag{9}$$

Since the curvature radius of the ring is much larger than the normal clearance, combined with Fig. 5(b), the bearing radial clearance c_{rj}' at the j-th ball position can be approximately expressed as:

$$c_{rj}' = \frac{\Delta_j}{\cos\alpha_j} = \frac{r_i + r_o - d_b - \sqrt{\left(\left|\overrightarrow{D_i O_{ij}'}\right|\right)^2 + \left(\left|\overrightarrow{O_{oj} D_i}\right|\right)^2}}{\cos\left[\arctan\left(\frac{\left|\overrightarrow{D_i O_{ij}'}\right|}{\left|\overrightarrow{O_{oj} D_i}\right|}\right)\right]} \tag{10}$$

Substituting Eqs. (3) and (7) into Eqs. (8)-(10), the expressions of the contact angle and bearing clearance of the

j-th ball caused by misalignment can be derived.

On this basis, the misalignment angle φ_y of the rotating axis along the Y-axis is introduced. Then Eqs. (3) and (4) can be further rewritten as:

$$\left|\overrightarrow{D_{\mathrm{i}}O_{ij}'}\right| = \left(r_{\mathrm{b}} + r_{\mathrm{i}}\right)\left[\sin\theta_j \sin\varphi_x - \cos\theta_j \sin\varphi_y\right] \tag{11}$$

$$\left|\overrightarrow{D_{\mathrm{i}}O_{ij}}\right| = (r_{\mathrm{b}} + r_{\mathrm{i}})\sqrt{\sin^2\theta_j(1-\cos\varphi_x)^2 + \cos^2\theta_j(1-\cos\varphi_y)^2} \tag{12}$$

Substituting Eq. (12) back into Eqs. (6) and (7), the result is as follows:

$$\left|\overrightarrow{O_{\mathrm{o}j}D_{\mathrm{i}}}\right| = \sqrt{\begin{array}{l}\left[(r_{\mathrm{i}} + r_{\mathrm{o}} - d_{\mathrm{b}} - c_{\mathrm{r}})\cos\theta_j\right]^2 + \\ \left[(r_{\mathrm{i}} + r_{\mathrm{o}} - d_{\mathrm{b}} - c_{\mathrm{r}})\sin\theta_j - (r_{\mathrm{b}} + r_{\mathrm{i}})\sqrt{\sin^2\theta_j(1-\cos\varphi_x)^2 + \cos^2\theta_j(1-\cos\varphi_y)^2}\right]^2\end{array}} \tag{13}$$

Then substitute Eqs. (2), (11) and (13) into Eqs. (8) and (10). Therefore, when the inner ring of the bearing tilts along any direction, the generalized expression of the contact angle and bearing clearance is as follows:

$$\alpha_j = \arctan\left(\frac{\left(r_{\mathrm{b}} + f_{\mathrm{i}}d_{\mathrm{b}}\right)\zeta}{\sqrt{\left(\chi - c_{\mathrm{r}}\right)^2\cos^2\theta_j + \left[(\chi - c_{\mathrm{r}})\sin\theta_j - (r_{\mathrm{b}} + f_{\mathrm{i}}d_{\mathrm{b}})\eta\right]^2}}\right) \tag{14}$$

$$\Delta_j = \chi - \sqrt{\left(r_{\mathrm{b}} + f_{\mathrm{i}}d_{\mathrm{b}}\right)^2\zeta^2 + \left(\chi - c_{\mathrm{r}}\right)^2\cos^2\theta_j + \left[(\chi - c_{\mathrm{r}})\sin\theta_j - (r_{\mathrm{b}} + f_{\mathrm{i}}d_{\mathrm{b}})\eta\right]^2} \tag{15}$$

$$c_{\mathrm{r}j}' = \frac{\chi - \sqrt{\left(r_{\mathrm{b}} + f_{\mathrm{i}}d_{\mathrm{b}}\right)^2\zeta^2 + \left(\chi - c_{\mathrm{r}}\right)^2\cos^2\theta_j + \left[(\chi - c_{\mathrm{r}})\sin\theta_j - (r_{\mathrm{b}} + f_{\mathrm{i}}d_{\mathrm{b}})\eta\right]^2}}{\cos\left[\arctan\left(\frac{\left(r_{\mathrm{b}} + f_{\mathrm{i}}d_{\mathrm{b}}\right)\zeta}{\sqrt{\left(\chi - c_{\mathrm{r}}\right)^2\cos^2\theta_j + \left[(\chi - c_{\mathrm{r}})\sin\theta_j - (r_{\mathrm{b}} + f_{\mathrm{i}}d_{\mathrm{b}})\eta\right]^2}}\right)\right]} \tag{16}$$

where,

$$\chi = (f_{\mathrm{i}} + f_{\mathrm{o}} - 1)d_{\mathrm{b}} \tag{17}$$

$$\zeta = \sin\theta_j \sin\varphi_x - \cos\theta_j \sin\varphi_y \tag{18}$$

$$\eta = \sqrt{\sin^2\theta_j(1-\cos\varphi_x)^2 + \cos^2\theta_j(1-\cos\varphi_y)^2} \tag{19}$$

Further, according to Ref [45,46], since the outer ring of bearing is matched with the bearing seat, the outer ring does not rotate. At this time, the rotational angular velocity of the bearing cage can be written as:

$$\omega_{\mathrm{c}} = \frac{\omega_{\mathrm{r}} r_{\mathrm{b}}}{R_{\mathrm{b}} + r_{\mathrm{b}}} \tag{20}$$

where, ω_{r} is the rotational angular velocity of the rotor. Due to the existence of pocket clearance in the cage, the angular position of each ball bearing is non-uniform distribution. Therefore, the angular position θ_j of the j-th ball

bearing can be expressed as:

$$\theta_j = \omega_c t + \frac{2\pi}{N_b}(j-1) + \theta_{01} + 2\tau_j \arcsin(\frac{c_c}{2d_m}) \tag{21}$$

In Eq. (21), the initial position angle of the first ball is θ_{01}, and τ_j is a random number evenly distributed between -1 and 1 (j=1,2,……,N_b). Further, in the initial misalignment state, the geometric relationship after bearing movement is shown in Fig. 6. The contact point between the j-th ball and the inner raceway changes from O_{ij}' to O_{ij}''. The distance between the curvature center of the inner and outer raceway after initial misalignment is A_j, and the distance between the curvature center of the inner and outer raceway after vibration is A_j'. Then the contact deformation δ_j between the j-th ball and the raceway can be written as:

$$\delta_j = \left|\overrightarrow{O_{oj}O_{ij}''}\right| - \left|\overrightarrow{O_{oj}O_{ij}'}\right| = A_j' - A_j \tag{22}$$

where,

$$A_j = \chi - \Delta_j \tag{23}$$

$$A_j' = \sqrt{\left(A_j \cos\alpha_j + \delta_{rj}\right)^2 + \left(A_j \sin\alpha_j + \delta_{zj}\right)^2} \tag{24}$$

The contact angle α_j' of the bearing after vibration can be written as follows:

$$\alpha_j' = \arctan\left(\frac{A_j \sin\alpha_j + \delta_{zj}}{A_j \cos\alpha_j + \delta_{rj}}\right) \tag{25}$$

In Eqs. (24) and (25), δ_{rj} and δ_{zj} are radial and axial contact deformations respectively, which can be expressed as follows:

$$\delta_{rj} = x\cos\theta_j + y\sin\theta_j - c_{rj}' \tag{26}$$

$$\delta_{zj} = z + r_{dj}\left(\theta_x \sin\theta_j - \theta_y \cos\theta_j\right) \tag{27}$$

Therefore, according to the Hertz contact theory, the expression of 5-DOF nonlinear bearing force considering deep groove ball bearing misalignment and cage pocket clearance is [47,48]:

$$\begin{cases} F_{\mathrm{b}x} = -\sum_{j=1}^{N_\mathrm{b}} k_{\mathrm{b}j}\delta_j^{1.5}\mathrm{H}(\delta_j)\cos\alpha_j'\cos\theta_j \\ F_{\mathrm{b}y} = -\sum_{j=1}^{N_\mathrm{b}} k_{\mathrm{b}j}\delta_j^{1.5}\mathrm{H}(\delta_j)\cos\alpha_j'\sin\theta_j \\ F_{\mathrm{b}z} = -\sum_{j=1}^{N_\mathrm{b}} k_{\mathrm{b}j}\delta_j^{1.5}\mathrm{H}(\delta_j)\sin\alpha_j' \\ M_{\mathrm{b}x} = -r_{\mathrm{d}j}\sum_{j=1}^{N_\mathrm{b}} k_{\mathrm{b}j}\delta_j^{1.5}\mathrm{H}(\delta_j)\sin\alpha_j'\sin\theta_j \\ M_{\mathrm{b}y} = r_{\mathrm{d}j}\sum_{j=1}^{N_\mathrm{b}} k_{\mathrm{b}j}\delta_j^{1.5}\mathrm{H}(\delta_j)\sin\alpha_j'\cos\theta_j \end{cases} \tag{28}$$

where, H(δ_j) is Heaviside function. $r_{\mathrm{d}j}$ represents the radial distance of the curvature center of the inner raceway at the j-th ball position. $k_{\mathrm{b}j}$ is the Hertz contact stiffness between the j-th ball and raceway. Their expressions are shown as follows [2,46-48]:

$$\mathrm{H}(\delta_j) = \begin{cases} 1, & \delta_j > 0 \\ 0, & else \end{cases} \tag{29}$$

$$r_{\mathrm{d}j} = 0.5d_\mathrm{m} + \left(f_\mathrm{i} - 0.5\right)d_\mathrm{b}\cos\alpha_j \tag{30}$$

$$k_{\mathrm{b}j} = \left\{\left[2.1458\times10^5\sum\rho_e^{-0.5}(\lambda_e^*)^{-1.5}\right]^{-\frac{2}{3}} + \left[2.1458\times10^5\sum\rho_e^{-0.5}(\lambda_e^*)^{-1.5}\right]^{-\frac{2}{3}}\right\}^{-1.5}, e = \mathrm{in}/\mathrm{out} \tag{31}$$

$$\begin{cases} \sum\rho_{\mathrm{in}} = \dfrac{1}{d_\mathrm{b}}\left(4 - \dfrac{1}{f_\mathrm{i}} + \dfrac{2\gamma}{1-\gamma}\right) \\ \sum\rho_{\mathrm{out}} = \dfrac{1}{d_\mathrm{b}}\left(4 - \dfrac{1}{f_\mathrm{o}} - \dfrac{2\gamma}{1+\gamma}\right) \end{cases}, \quad \gamma = \frac{d_\mathrm{b}\cos\alpha_j}{d_\mathrm{m}} \tag{32}$$

In Eqs. (31) and (32), $\sum\rho_k$ represents the sum of inner/outer raceway curvature, and the parameters can also be obtained according to Ref [2].

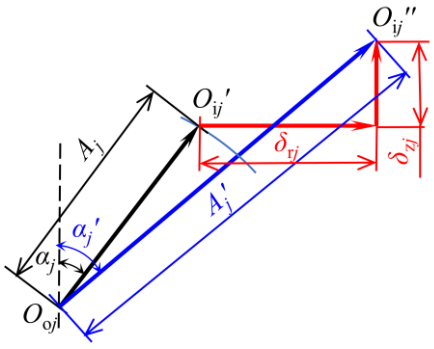

Fig. 6 Geometric deformation relationship of bearing after movement

2.2. Misalignment model of coupling

The diagram of coupling misalignment is shown in Fig. 7, in which points O_1 and O_2 are the rotation centers of right halve-coupling and left halve-coupling, respectively, and points O and P are the static center and dynamic center of the coupling housing, respectively. δ represents the misalignment of the coupling. When misalignment fault exists in the coupling, an additional exciting force, F_c, will be applied to the rotor system. If the exciting force F_c is projected onto the OXY coordinate system, its component can be expressed as [21,23,26]:

$$\begin{cases} F_{cx} = 2m_c\delta\omega_r^2 \sin\left(2\omega_r t\right) \\ F_{cy} = 2m_c\delta\omega_r^2 \cos\left(2\omega_r t\right) \end{cases} \tag{33}$$

where, m_c is the coupling mass, and the coupling misalignment δ can be expressed as follows:

$$\delta = \Delta l \tan\varphi + \Delta e \tag{34}$$

in Eq. (34), Δl is the distance between two coupling halves, Δe represents the parallel misalignment of the coupling. In this paper, Δe =0.

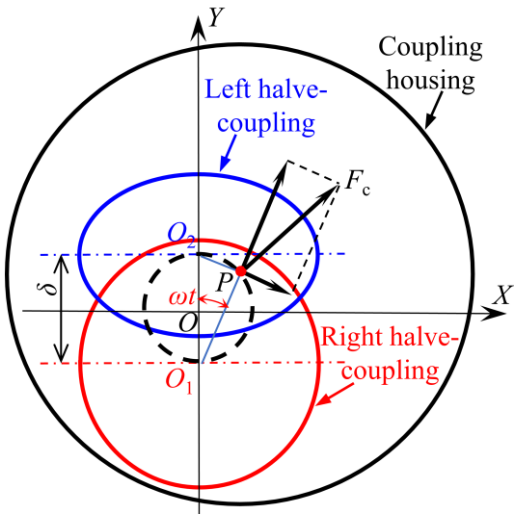

Fig.7 Schematic of coupling misalignment model

2.3. Finite element model of rotor system

According to Timoshenko beam element theory, each divided shaft element contains two nodes, as shown in Fig. 2 (b). The i-th node has 6 DOFs, and the displacement and rotation angles of node i in X, Y and Z directions are denoted by x_i, y_i, z_i, θ_{xi}, θ_{yi} and θ_{zi}, respectively. Therefore, the displacement vector of the q-th shaft element can be written as:

$$\boldsymbol{U}_q = [x_i, y_i, z_i, \theta_{xi}, \theta_{yi}, \theta_{zi}, x_{i+1}, y_{i+1}, z_{i+1}, \theta_{xi+1}, \theta_{yi+1}, \theta_{zi+1}]^{\mathrm{T}} \tag{35}$$

According to Ref. [49], the mass matrix $\boldsymbol{M}_{sq}$, stiffness matrix $\boldsymbol{K}_{sq}$ and gyro matrix $\boldsymbol{J}_{sq}$ of the q-th shaft element can be further determined. The mass matrix $\boldsymbol{M}_s$, stiffness matrix $\boldsymbol{K}_s$ and gyro matrix $\boldsymbol{J}_s$ of the rotating shaft can be obtained through the assembly of elements. The damping matrix $\boldsymbol{C}_s$ of the rotor system is determined in the form

of proportional damping [49]. In addition, gyro matrix $\boldsymbol{D}_{dp}$ and mass matrix $\boldsymbol{M}_{dp}$ of the disc element at the p-th node can be written as follows:

$$\boldsymbol{D}_{dp}=\begin{bmatrix}0&0&0&0&0&0\\0&0&0&0&0&0\\0&0&0&0&0&0\\0&0&0&0&J_{pp}&0\\0&0&0&-J_{pp}&0&0\\0&0&0&0&0&0\end{bmatrix},\quad \boldsymbol{M}_{dp}=\operatorname{diag}\left\{m_{dp},m_{dp},m_{dp},J_{dp},J_{dp},J_{pp}\right\},\quad p=11,18 \tag{36}$$

In Eq. (36), the mass, diameter moment of inertia and polar moment of inertia of the disc are m_{dp}, J_{dp} and J_{pp} respectively, which can be calculated according to the disc material density and the geometry (inner radius r_d, outer radius R_d and thickness h_d) in Fig. 2 (c):

$$m_{dp}=\pi\rho h_d\left(R_d-r_d\right)^2,\quad J_{dp}=\frac{\pi\rho h_d\left(R_d-r_d\right)^4}{4},\quad J_{pp}=\frac{\pi\rho h_d\left(R_d-r_d\right)^4}{2} \tag{37}$$

By assembling the disc mass matrix and gyro matrix at rotor nodes 11 and 18, the overall disc mass matrix $\boldsymbol{M}_d$ and gyro matrix $\boldsymbol{J}_d$ are obtained. Therefore, the differential equation of motion of the rotor system has the following form:

$$\left(\boldsymbol{M}_s+\boldsymbol{M}_d\right)\ddot{\boldsymbol{U}}+\left[\boldsymbol{C}_s+\omega_r\left(\boldsymbol{J}_s+\boldsymbol{J}_d\right)\right]\dot{\boldsymbol{U}}+\boldsymbol{K}_s\boldsymbol{U}=\boldsymbol{F}_b+\boldsymbol{F}_c+\boldsymbol{F}_e-\boldsymbol{G} \tag{38}$$

where, $\boldsymbol{U}$ is the displacement vector of the rotor system. $\boldsymbol{F}_c$ is the misalignment force vector of the coupling. $\boldsymbol{F}_e$ and $\boldsymbol{F}_b$ represent the unbalance force and rolling bearing force vector, respectively. $\boldsymbol{G}$ is the gravity vector of the rotor system. Assuming that the unbalance of the system exists only on two discs, the rotor unbalance force can be written as:

$$\begin{cases}F_{epx}=m_{dp}e_{dp}\omega_r^2\cos\omega_r t\\F_{epy}=m_{dp}e_{dp}\omega_r^2\sin\omega_r t\end{cases},\quad p=11,18 \tag{39}$$

where, F_{epx} and F_{epy} are the components of the unbalance force in the X/Y direction respectively, and e_{dp} is the eccentric distance at the disc P. It is known that the density of the rotor system is 7806 kg/m^3, the elastic modulus is 211 GPa, and the Poisson's ratio is 0.3. In addition, the length and diameter of each shaft element of the rotor are shown in Table 1. The parameters of the rolling bearings supported at both ends of the rotor are shown in Table 2.

Table 1 Parameters of the rotating shaft

Number of shaft element	Length of shaft element/mm	Diameter of shaft element/mm	Number of shaft element	Length of shaft element/mm	Diameter of shaft element/mm
1	6	16	13-15	40	30
2	15	16	16	40	30

3	20	16	17	25	50
4	20	16	18	5	50
5	16.5	25	19	23	30
6	15	25	20-22	40	30
7	7.5	25	23	7.5	25
8	25	30	24	15	25
9	27	30	25	16.5	25
10	5	50	26	15	18
11	25	50	27	10	18
12	30	30			

Table 2 Parameters of the deep groove ball bearing

Parameter	Value
Type	6205
Radius of inner raceway r_b/mm	15.55
Radius of outer raceway R_b/mm	23.49
Ball diameter d_b/mm	7.938
Ball number N_b	9
Initial radial clearance c_r/μm	8
Curvature radius coefficient of inner\outer raceway f_i\f_o	0.515
Initial contact angle α_0/°	0

3. Dynamic response analysis of the system

In this paper, the Newmark-β numerical integration method is used to solve Eq. (38), and each calculation period is further divided into 512 integration steps. After extracting the calculated data of the last 100 cycles, the dynamic characteristics of the ball bearing-coupling-rotor system with angular misalignment fault are analyzed through the rotor orbit, time-domain waveform, FFT frequency spectrum and Poincaré section map.

3.1. Comparison of system vibration response between Case 1, Case 2 and Case 3

In the traditional research on rotor misalignment, most of the references only consider coupling misalignment. This paper assumes that the coupling misalignment is Case 1, as shown in Fig. 8(a). The single consideration of bearing misalignment is Case 2, as shown in Fig. 8(b). As considered in this paper, the combined misalignment between coupling and bearing is Case 3, as shown in Fig. 2(a). It is assumed that there is only misalignment $\varphi=\varphi_x=0.2°$ in the direction around the X-axis. In the whole speed-raising process ($n\in$[2000, 15000]r/min) of the system under the three cases, the spectrum cascade at the left disc (node 11) is shown in Fig. 9. It can be seen from the figure that in all three cases, the system is mainly excited by rotating frequency (f_r) caused by rotor unbalance. For case 1 and case 3, there is also a tiny amount of $2f_r$ caused by coupling misalignment excitation in the spectrum, while case 2 has no such frequency. By comparison, it can also be found that the critical speed of the rotor system in Case 1 is about 11600 r/min, while the critical speed is increased to about 11800 r/min in Case

2 and Case 3. This is because after considering the bearing misalignment, the support stiffness of bearing to the rotor increases, thus increasing the natural frequency of the system.

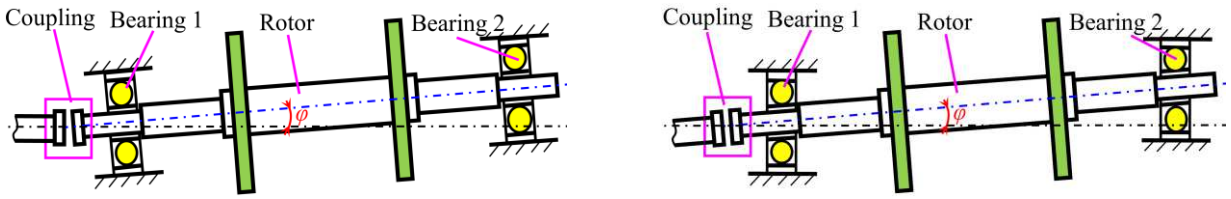

(a) (b)

Fig. 8 Misalignment of rolling bearing rotor system: (a) Case 1 (coupling misalignment), and (b) Case 2 (bearing misalignment)

Figure 10 presents the radial (*X*/*Y*-direction) spectrum cascade of the left disc under three cases when the rotor is operating in the low-speed range ($n \in [2000, 5000]$ r/min). For case 1, the frequency components of f_r and its super harmonic are appeared in both *X*- and *Y*-directions. With the increase of rotating speed, the amplitude of $2f_r$ increases most obviously. For Cases 2 and 3, it can be obviously found that in addition to f_r and its super harmonic components, the frequency component of bearing varying compliance vibration (f_{vc}) also appears, which indicates that the misalignment can aggravate the bearing varying compliance (VC) vibration in the low-speed range. In addition, under the combined action of VC vibration of bearing and unbalanced vibration of the rotor, the combined frequency components of f_{vc} and f_r appear in the spectrum, such as f_{vc}-f_r, f_{vc}-$2f_r$, $4f_r$-$3f_{vc}$ and so on. However, with the gradual increase of rotational speed, the influence of rotor unbalance vibration excitation increases gradually, and the vibration frequency of f_{vc} weakens and disappears gradually when the rotational speed is higher than 4000r/min. In addition, it can also be found that for Cases 2 and 3 with bearing misalignment, the frequency amplitude in the *X*-direction is larger than that in the *Y*-direction. This is mainly because when there is a bearing misalignment around the *X*-axis of the system, the constraint of the bearing on the rotor in the *Y*-direction enhances and the rotor deflection increases. It can be seen that the bearing misalignment has a strong directivity. For Case 3, under the combined action of misalignment of coupling and bearing, it can be found that compared with Case 1, bearing misalignment can cause the occurrence of f_{vc} and the combined frequency components of f_{vc} and f_r in the system. Compared with bearing misalignment (Case 2), coupling misalignment further causes frequency $2f_r$ of the system.

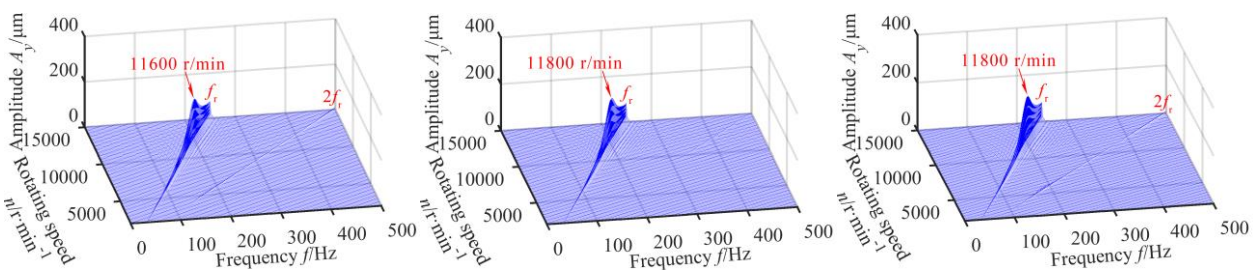

(a) (b) (c)

Fig.9 Spectrum cascade of speed up under different cases: (a) Case 1, (b) Case 2, and (c) Case 3

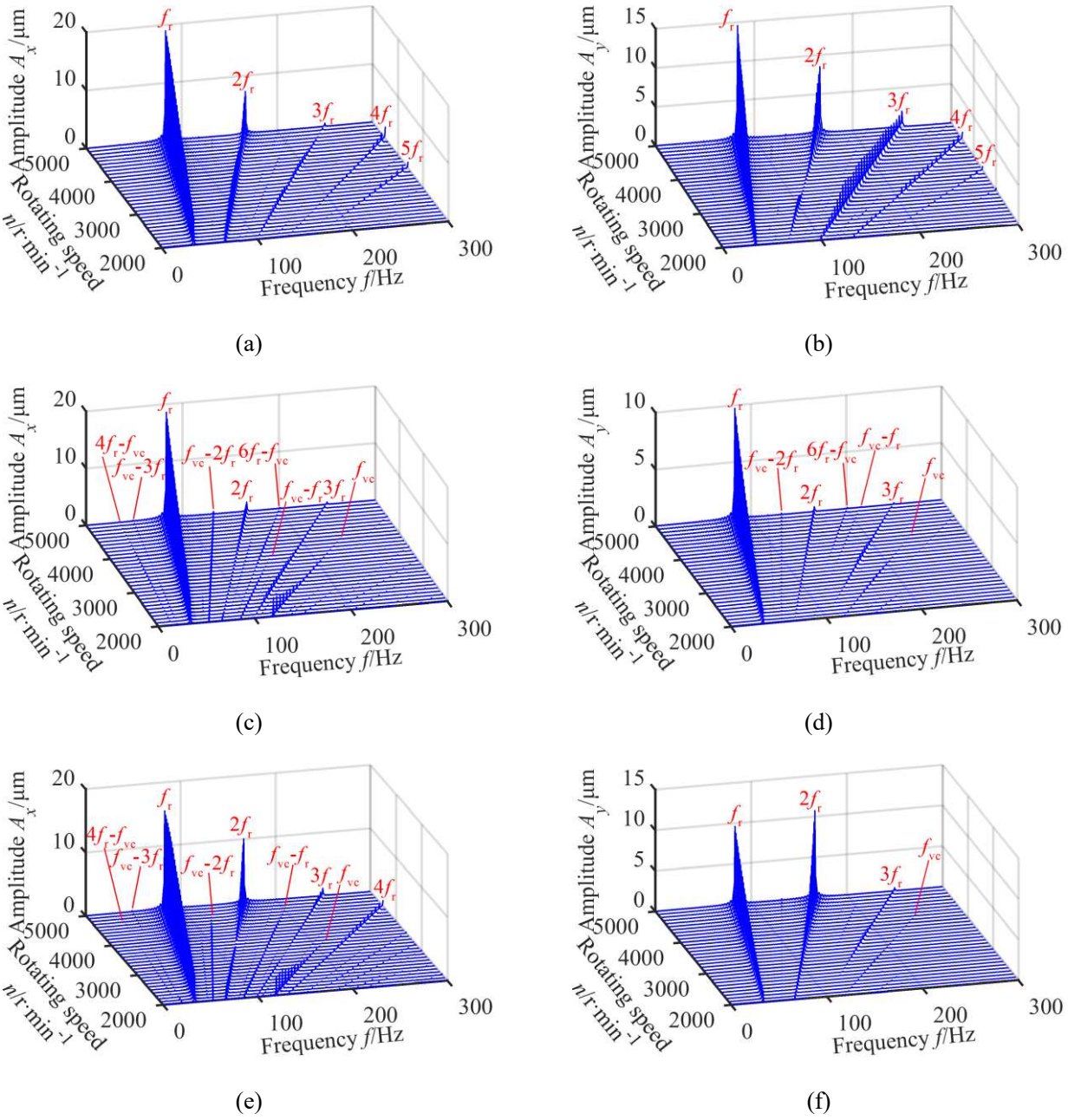

Fig. 10 Spectrum cascade of rotor in low-speed range: (a) Case 1, *X*-direction, (b) Case 1, *Y*-direction, (c) Case 2, *X*-direction, (d) Case 2, *Y*-direction, (e) Case 3, *X*-direction, and (f) Case 3, *Y*-direction

Taking the vibration response of the rotor system under the operation of 2000 r/min and 6000 r/min as an example, the results are shown in Figs. 11 and 12, respectively. Through further comparison, the similarities and differences of the three misalignments are shown as follows:

(1) When the rotating speed is n=2000 r/min, the vibration responses of Cases 1, 2 and 3 are pretty different. For radial vibration, combined with Figs. 11(a) and (b), it can be found that in Case 1, the rotating speed is low, and the effect of rotor unbalance is weak. Due to the existence of gravity, the vibration center of the rotor is

located in the negative direction of the *Y*-axis. After considering the bearing misalignment, the motion trajectory of the rotor has an apparent upward trend. This is due to the misalignment assumed in this paper as shown in Fig. 2, the right end of the rotor is "lifted" upward. Therefore, further consideration of the misalignment of the rotor support can better simulate the misalignment problem assumed in this paper. Figure 11(d) also clearly shows that, compared with Case 2 of bearing misalignment, considering Case 1 and Case 3 of coupling misalignment can make the frequency component of $2f_r$ in the system more obvious. Compared with Case 1 of coupling misalignment, considering Cases 2 and 3 of bearing misalignment can make the frequency component of f_{vc} in the system more obvious. In addition, there exist abundant combination frequency components, such as $nf_{vc}\pm mf_r$ (n and m are positive integers).

(2) For axial vibration, only the coupling misalignment will not generate axial excitation, so the axial vibration in Case 1 is very small and can be almost negligible. When the bearing misalignment is further considered, the misalignment makes the bearing produce a component force along the axial direction, which leads to the increase of the axial vibration of the system under the action of this excitation. In addition, misalignment also results in a constant component of rotor gravity along *Z*-direction, so the balance position of vibration waveform in this direction is located in the negative direction of the *Z*-axis, as shown in Fig. 11(c). Under the action of bearing misalignment, except that f_{vc} and corresponding combined frequency components will still be generated in Case 2 and Case 3, the rotor unbalance generated in the radial direction and the coupling misalignment in Case 3 will generate frequencies such as f_r and $2f_r$ in the FFT spectrum of the axial direction, as shown in Fig. 11(e).

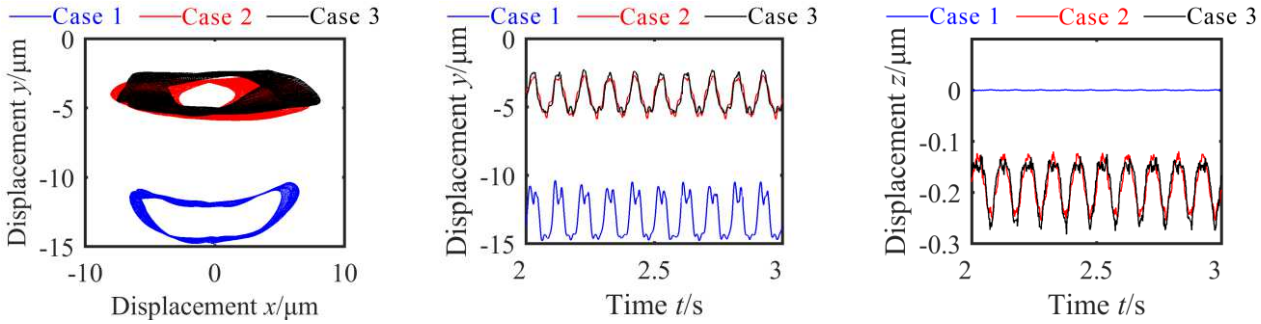

(a) (b) (c)

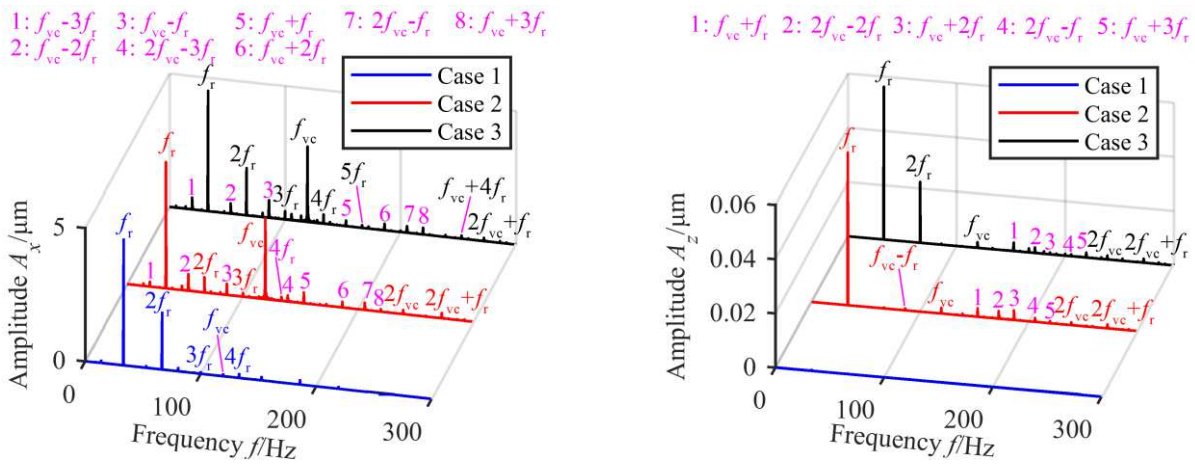

Fig.11 Comparison of three cases at rotating speed n=2000r/min: (a) rotor orbit, (b) time-domain waveform of radial direction, (c) time-domain waveform of axial direction, (d) FFT spectrum of radial direction, and (e) FFT spectrum of axial direction

(3) As can be seen from Fig. 12, when the speed n=6000 r/min, the rotor orbits of Cases 1 and 3 with coupling misalignment fault both show the motion law of two ellipses nested with each other, and the time-domain waveforms present the feature of alternating high and low peaks, and the amplitudes of f_r and 2f_r in the spectrum are prominent. However, for Case 2, the rotor orbit presents an elliptical shape, the vibration waveform is approximately a sine wave, and the frequency f_{vc} gradually weakens and disappears in the end. These characteristics show that the system vibration is mainly excited by rotor unbalance and coupling misalignment after the speed increases, and the bearing misalignment has little effect. This is because rotor unbalance force and coupling misalignment force are related to the square term of rotating speed according to Eqs. (33) and (39), while bearing misalignment force is only related to the first power of rotor speed. Therefore, with the enhance of rotating speed, the increase of rotor unbalance force and coupling misalignment force is much greater than that of bearing misalignment force. It can be seen that the influence of rotor unbalance and coupling misalignment on the system at high speed is greater than that of bearing misalignment. For axial vibration, the amplitude of Cases 2 and 3 with bearing misalignment is greater than Case 1. The axial vibration under bearing misalignment (Case 2) is approximately sine wave. The amplitude of Case 3 combined with coupling misalignment and bearing misalignment is greater than that of Case 2 with bearing misalignment only. The axial waveform under Case 3 shows the vibration characteristics of alternating high and low peaks, and the amplitude of 2f_r in the spectrum is slightly higher than that of f_r.

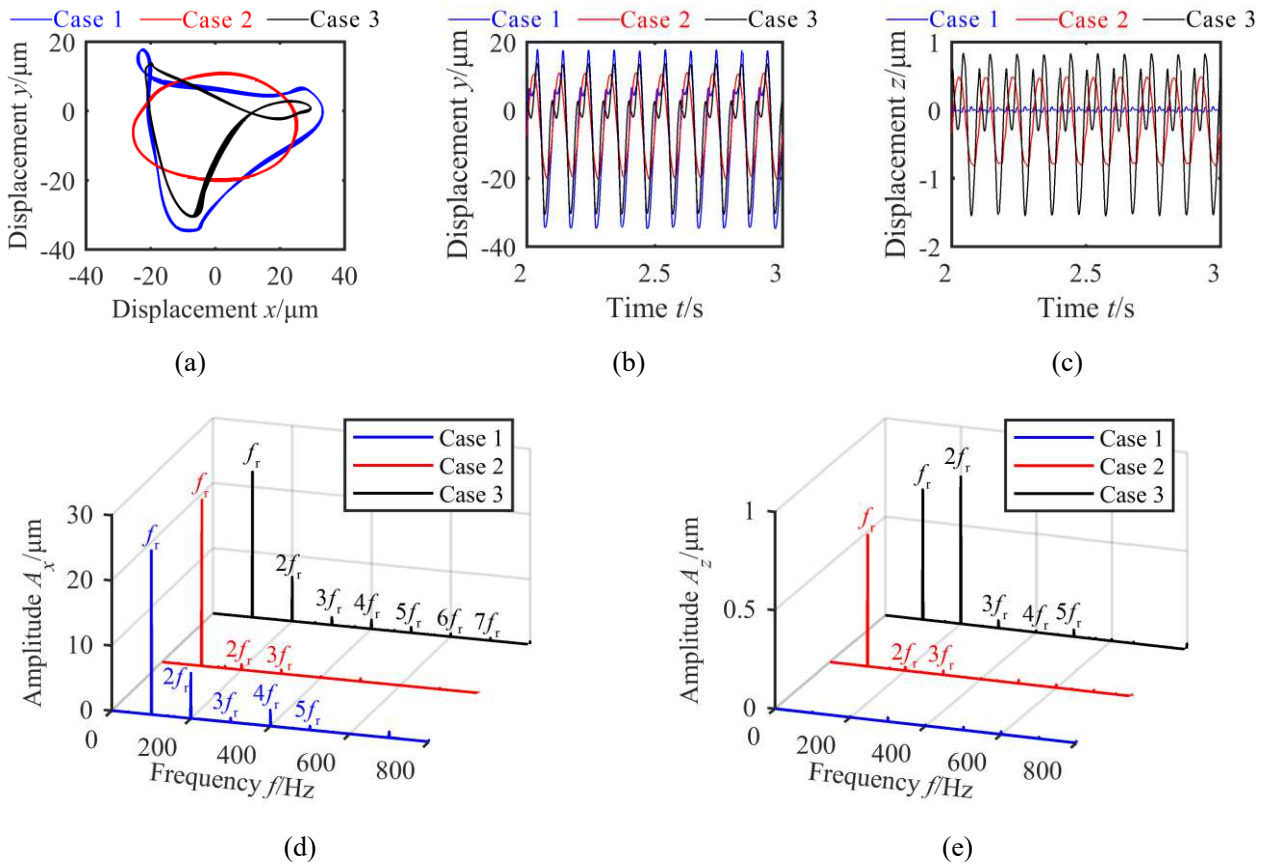

Fig.12 Comparison of three cases at rotating speed n=6000r/min: (a) rotor orbit, (b) time-domain waveform of radial direction, (c) time-domain waveform of axial direction, (d) FFT spectrum of radial direction, and (e) FFT spectrum of axial direction

To sum up, in the low-speed range, the bearing misalignment has a significant influence on the dynamic characteristics of the rotor system, while the coupling misalignment has a relatively small influence. At this time, there is little difference in the system dynamic characteristics between Case 2 and Case 3. Therefore, for the rotor misalignment discussed in this paper, the factor of bearing misalignment cannot be ignored. In terms of frequency characteristics, bearing misalignment increases the amplitude of VC frequency (f_{vc}), and the combined frequency of f_{vc} and rotating frequency (f_r) is more abundant. The coupling misalignment increases the amplitude of $2f_r$. Bearing misalignment also increases the support stiffness of the rotor system, resulting in the increase of the critical speed of the system. Bearing misalignment also makes the vibration of the system have strong directivity. As the misalignment causes the bearing to produce a restoring component force along the axial direction, the axial vibration of the system increases under this excitation. In addition, because the rotor unbalance force and coupling misalignment force are related to the square term of rotating speed, while the bearing misalignment force is only related to the first power of speed. Therefore, the influence of bearing misalignment decreases gradually with the increase of rotating speed. The frequency components of f_{vc} and the combined frequency gradually weaken or even disappear. In contrast, the influence of rotor unbalance and coupling misalignment enhances gradually, and

the frequency components of f_r and $2f_r$ are obvious. At this time, there is little difference in the system dynamic characteristics between Cases 1 and 3.

3.2. Effect of misalignment degree

3.2.1. Process of speed-up

Based on the discussion in Section 3.1, this section takes Case 3 under the action of misalignment of coupling and bearing as an example to further discuss the influence of different misalignment degrees on the dynamic characteristics of the system in the process of speed-up. When the system is in a healthy state (φ=0°) and misaligned state (φ=0.2°) respectively, radial and axial amplitude curves at the left rotor disc (node 11) are shown in Fig. 13. It is not difficult to find the following interesting phenomena from the figure:

(1) For the radial vibration of the system, as shown in Fig. 13(a). Misalignment increases the critical speed of the system from about 11600 r/min to about 11830 r/min, indicating that bearing misalignment increases the support stiffness of the system, which is consistent with the conclusion obtained from the test results in Ref. [33]. In the subcritical speed range, the system amplitude decreases due to misalignment. The misalignment causes the system amplitude to increase slightly in the range of critical and supercritical speeds.

(2) For the axial vibration of the system, as shown in Fig. 13(b). The axial vibration is slightly in a healthy state. Misalignment intensifies the axial vibration of the system, and the resonance peak appears at about 11900 r/min. It can be seen that misalignment has a great influence on the axial vibration of the system. This shows that axial vibration is another basis for judging whether there is angular misalignment fault in the deep groove ball bearing-rotor system.

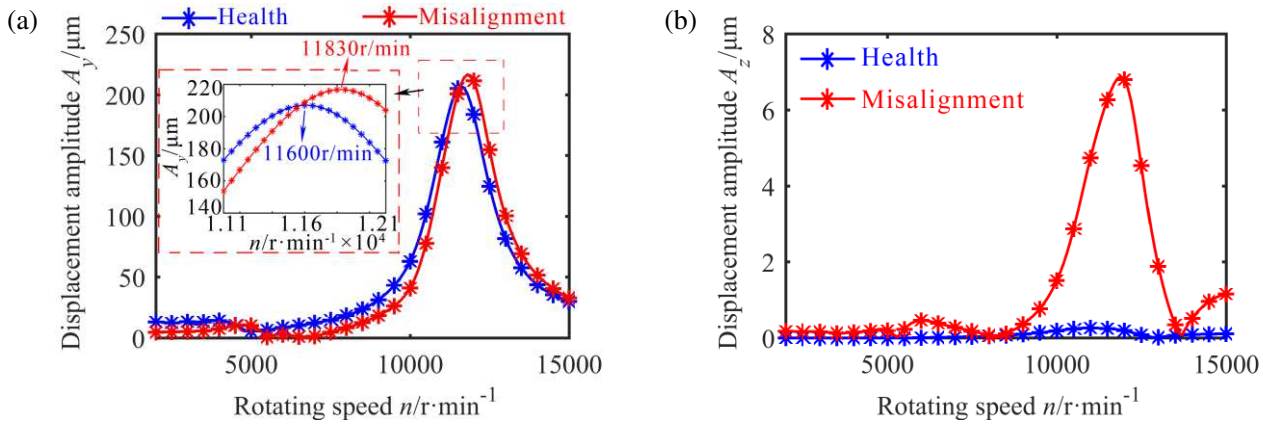

Fig. 13 System amplitude curve in the process of speed-up, (a) *Y*-direction and (b) *Z*-direction

3.2.2. Process of steady speed

Taking the No. 1 ball of the left bearing with rotating speed n=3000 r/min as an example, the influence laws of different misalignment on bearing parameters, such as contact angle, radial clearance, and ball

revolution angular velocity are shown in Fig. 14. When the system is in a healthy state (φ=0°), the contact angle α_j of deep groove ball bearing is always 0°. It can be seen from Table 2 and Fig. 14 (b) that the bearing radial clearance c_r is constant at 8 μm. The approximate calculation formula of the angular velocity of ball revolution is given as follows:

$$\omega_{bj}=\left(1-\frac{d_b}{d_m}\cos\alpha_j\right)\frac{\omega_r}{2} \tag{40}$$

By calculation, the rotational angular velocity ω_{bj} of each ball bearing in this state is constant at 125.1 rad/s. When a misalignment fault appears in the system, the misalignment makes the contact angle and radial clearance of each ball bearing no longer constant, but shows a law of periodic change. At each moment, all the ball contact angles of the bearing and the radial clearance at the position of the ball are not equal. Although the average value of the contact angle within one revolution is still 0 °, the contact angle of the ball fluctuates with approximate sinusoid. The bearing radial clearance fluctuates twice within the range of one rotation of the ball, which indicates that misalignment causes the bearing to have two contact areas with a central phase difference of 180°. With the increase of misalignment degree, the amplitude of this periodic fluctuation also increases gradually, and the average radial clearance decreases gradually. Under a significant misalignment, the bearing clearance may even be negative at a certain position of the ball rolling. This indicates that the bearing misalignment has squeezed some of the balls in the bearing. Combined with Eq. (40), the contact angles of the balls are not equal at all places on the circumference of the raceway, so the rotational angular velocity of each ball is constantly changing and unequal. The degree of difference between the angular velocity of each ball increases with the increase of misalignment. Taking the misalignment angle φ=0.21° as an example, according to Figs. 14(c) and (d), the maximum and minimum values of the ball angular velocity on the circumference are about 90° apart. In other words, when the ball is rotated 1/4 turn, the angular velocity increases by 1.5 rad/s. According to this calculation, the maximum velocity difference of ball revolution in the bearing can reach about 0.06 m/s. It can be seen that the relative tilt of bearing caused by rotor misalignment will lead to the unequal angular velocity of the ball and cage, and the center of the ball and cage pocket do not coincide. When the distance between the two centers is greater than the clearance of cage pocket c_c, an elastic collision occurs between the ball and the cage pocket. Moreover, the more serious the misalignment, the greater the impact strength of the ball on the cage along the circumferential direction, which improves the possibility of fatigue fracture of the cage.

According to Eqs. (22), (31) and (32), the contact force of the j-th ball can be calculated as $F_{bj}=k_{bj}\delta_j^{1.5}$. The maximum contact force max(F_{b1}) of the No. 1 ball in the time range of one revolution under different

misalignment conditions is extracted, respectively. It is also marked that the maximum contact force of the ball bearing without misalignment is max(F_{b1_0}). The relative variation of the maximum contact force of the ball under different misalignment degrees can be calculated according to the following equation:

$$\varepsilon = \frac{\max(F_{b1}) - \max(F_{b1\_0})}{\max(F_{b1\_0})} \times 100\% \tag{41}$$

The maximum contact force variation curve of the ball is calculated according to the Eq. (41), as shown in Fig. 15. With the misalignment angle increases, the contact force presents a trend of nonlinear increase. The more serious the misalignment, the more obvious the increase of the contact force between the ball and the raceway. When the misalignment angle φ=0.21°, the maximum contact force even increases by 183.6%. This may further lead to contact deformation between the ball and the raceway, which is not conducive to the stable operation of the bearing.

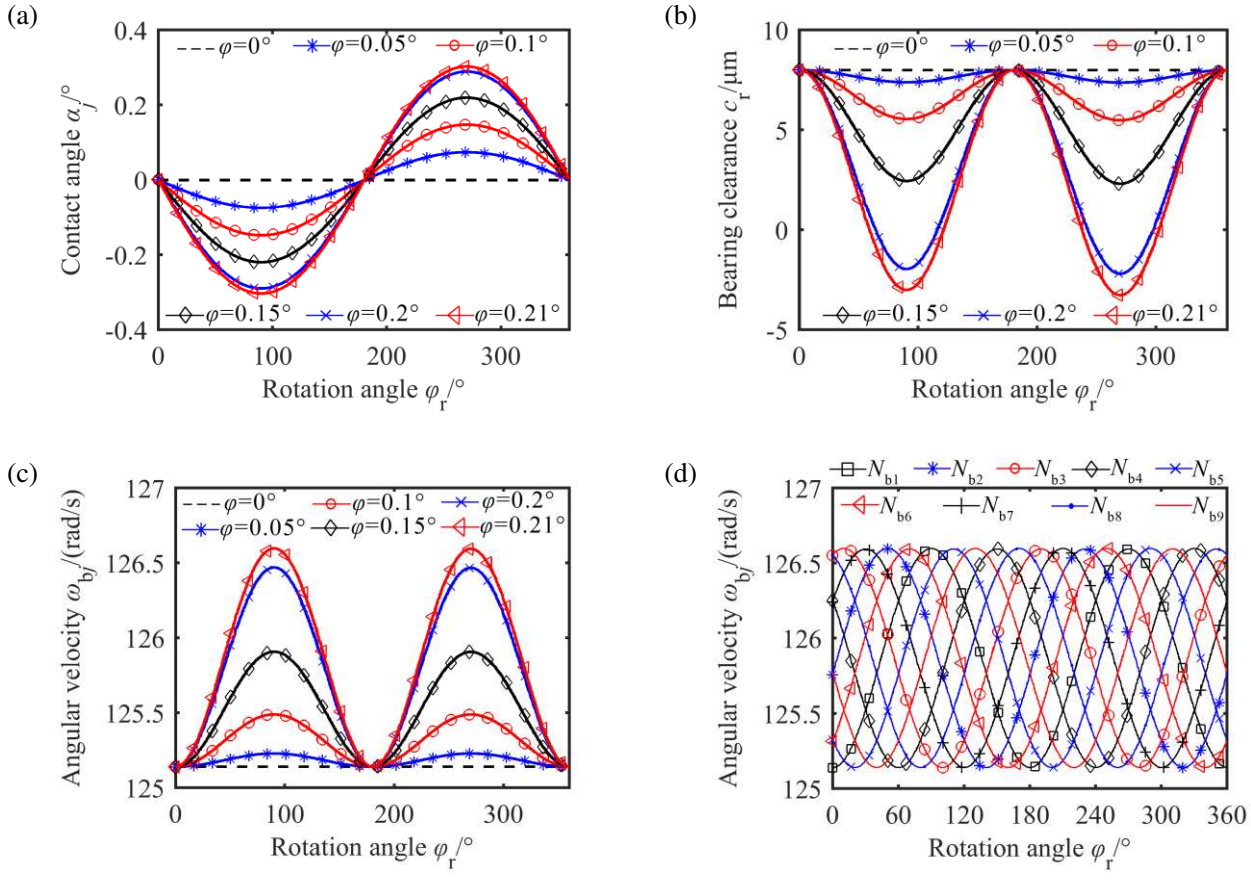

Fig. 14 Influence of misalignment on bearing parameters: (a) influence of misalignment degree on the contact angle of the No. 1 ball, (b) influence of misalignment degree on the radial clearance at the No. 1 ball, (c) influence of misalignment degree on the revolution angular velocity of the No. 1 ball, and (d) the angular velocity of different balls at misalignment degree φ=0.21 °

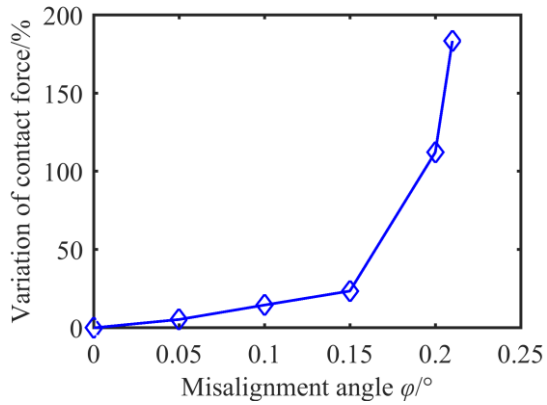

Fig. 15 Effect of misalignment on contact force of ball bearing

Next, the influence of misalignment on dynamic characteristics of the ball bearing-coupling-rotor system is further discussed. The variation range of misalignment angle is set as $\varphi \in [0, 0.21]°$. The vibration response of the left disc of the rotor under the subcritical speed range (n=3000 r/min), critical speed range (n=11830 r/min) and supercritical speed range (n=15000 r/min) is selected. The results are shown in Figs. 16-19. It is not difficult to find the following phenomena:

(1) When the rotor operates in the subcritical speed range (n=3000 r/min). Combined with Figs. 16 (a), (b) and Fig. 17, it can be seen that under the healthy state (φ=0°), the vibration center of the rotor under the action of gravity is in the negative direction of Y-direction due to the weak unbalance excitation of the rotor. The rotating frequency (f_r) and its higher harmonic components are the main components in the spectrum. With the increase of misalignment angle, the rotor orbit and time-domain waveform of Y-direction show the trend of upward translation. The radial amplitude decreases slightly, and the amplitude of frequency f_r and its super-harmonic components also decrease. The frequency amplitude of f_r decreases from 4.639 μm (φ=0°) to 2.913 μm (φ=0.21°). This is because the misalignment fault enhances the constraint of bearing on the rotor. With the further increase of misalignment angle, the frequency amplitude of $2f_r$ increases, resulting from the enhancement of coupling misalignment. The rotor system always keeps quasi-periodic motion under the condition of health and misalignment. In a healthy state, the axial vibration of the deep groove ball bearing-rotor system almost does not exist, and it increases gradually with the increase of misalignment degree. Specifically, the amplitude of f_r and its super-harmonic components increases, and the increase of f_r is the most obvious in the axial spectrum. In addition, the amplitude of VC frequency (f_{vc}) of bearing increases with the increase of misalignment, whether radial vibration or axial vibration. This indicates that misalignment intensifies the VC vibration of bearing.

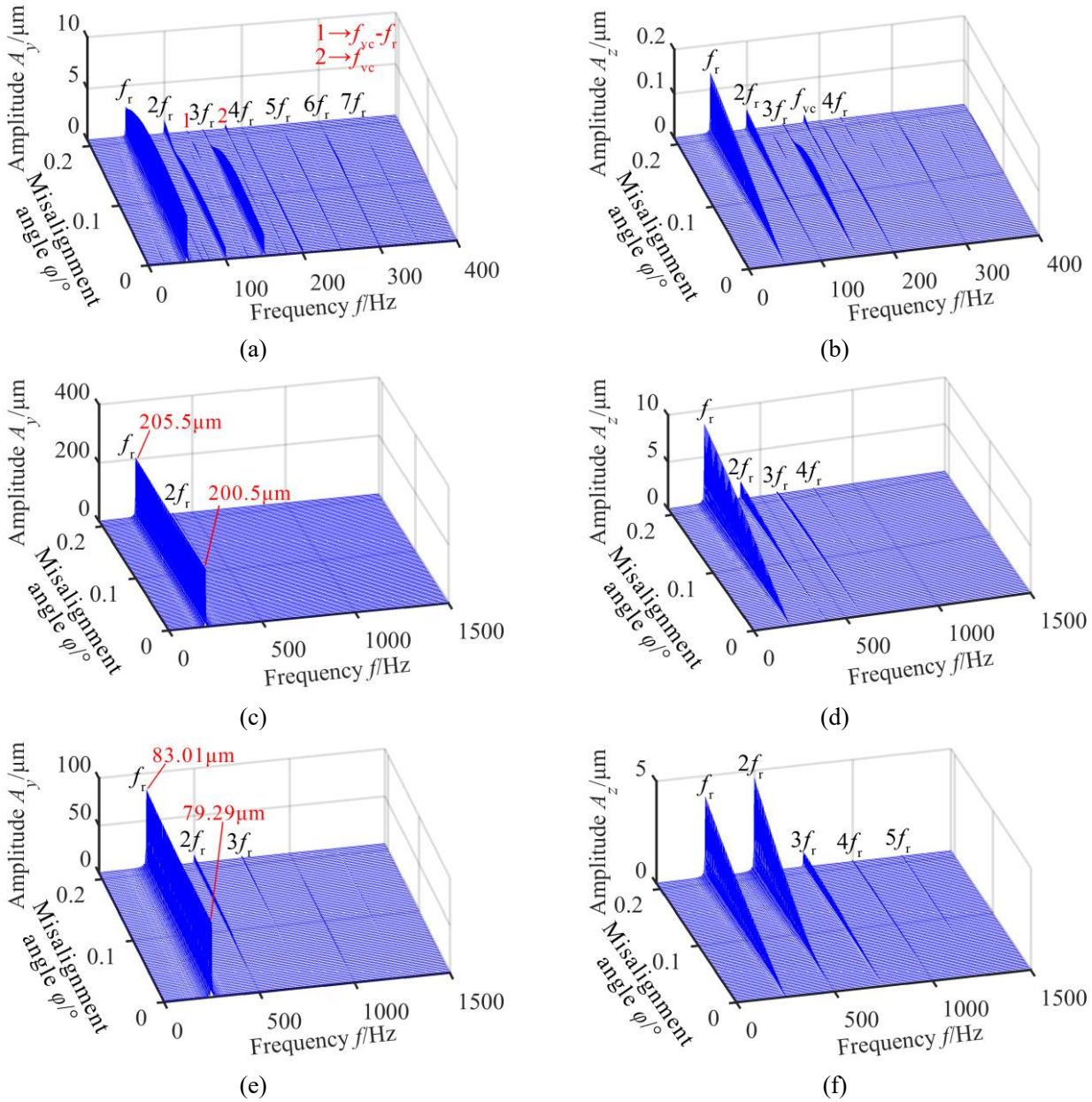

Fig. 16 Spectrum cascade of rotor system under different misalignment: (a) 3000 r/min, *Y*-direction, (b) 3000 r/min, *Z*-direction, (c) 11830 r/min, *Y*-direction, (d) 11830 r/min, *Z*-direction, (e) 15000 r/min, *Y*-direction, and (f) 15000 r/min, *Z*-direction

(2) When the rotor operates in the critical speed range (n=11830 r/min), it can be seen from Figs. 16 (c), (d) and Fig. 18 that the system amplitude increases sharply in the resonance state, and the system vibration is mainly excited by rotor unbalance. Under the action of unbalance excitation, the rotor orbit shows an elliptic curve before and after misalignment, and the time-domain waveforms of radial and axial directions are approximately sine waves. In the radial spectrum, the frequency of f_r caused by unbalance excitation is the main component, and the frequency amplitude of $2f_r$ caused by misalignment excitation is relatively low. At this time, the radial vibration of the rotor system is not affected by the misalignment. Only the frequency amplitude of f_r increases slightly from 200.5 μm (φ=0°) to 205.5 μm (φ=0.21°). In the critical speed range, the influence of misalignment on the axial

vibration of the rotor system is almost the same as that in the subcritical speed range. Then the rotor system runs stably under the period-one (P-1) motion state.

(3) When the rotor speed is further increased to the supercritical speed range (n=15000 r/min). Combined with Figs. 16(e), (f) and Fig. 19, it can be seen that after passing the critical speed range, the amplitude of system decreases although it is still in the P-1 motion state. In the radial vibration, the system is still dominated by rotor unbalance excitation. With the increase of misalignment degree, both the axial and radial amplitudes of the system increase, and the frequency amplitudes of f_r and its higher harmonic enhance. In the radial spectrum, the amplitude of f_r rises from 79.29 μm (φ=0°) to 83.01 μm (φ=0.21°). Under the influence of coupling misalignment excitation, the rotor orbit changes gradually from regular ellipse in the healthy state to triangle. The axial vibration waveform presents the characteristics of alternating vibration of high and low peaks. In the axial spectrum, the frequency amplitude of $2f_r$ increases even more than that of f_r.

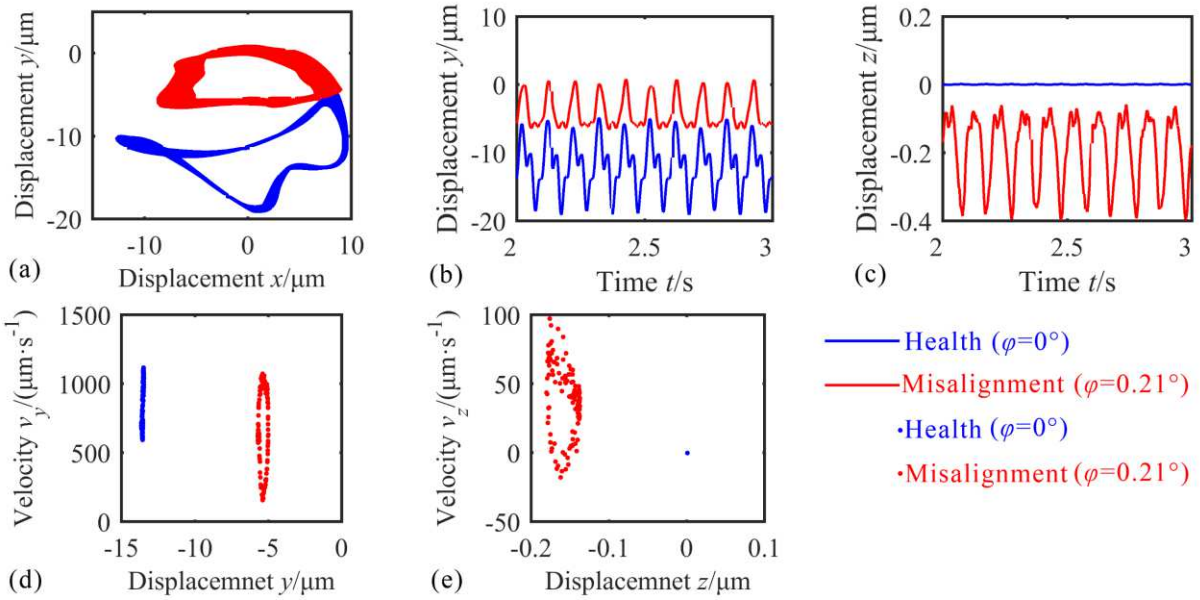

Fig. 17 System vibration response at n=3000r/min: (a) rotor orbit, (b) time-domain waveform in Y-direction, (c) time-domain waveform in Z-direction, (d) Poincaré section map in Y-direction and (e) Poincaré section map in Z-direction

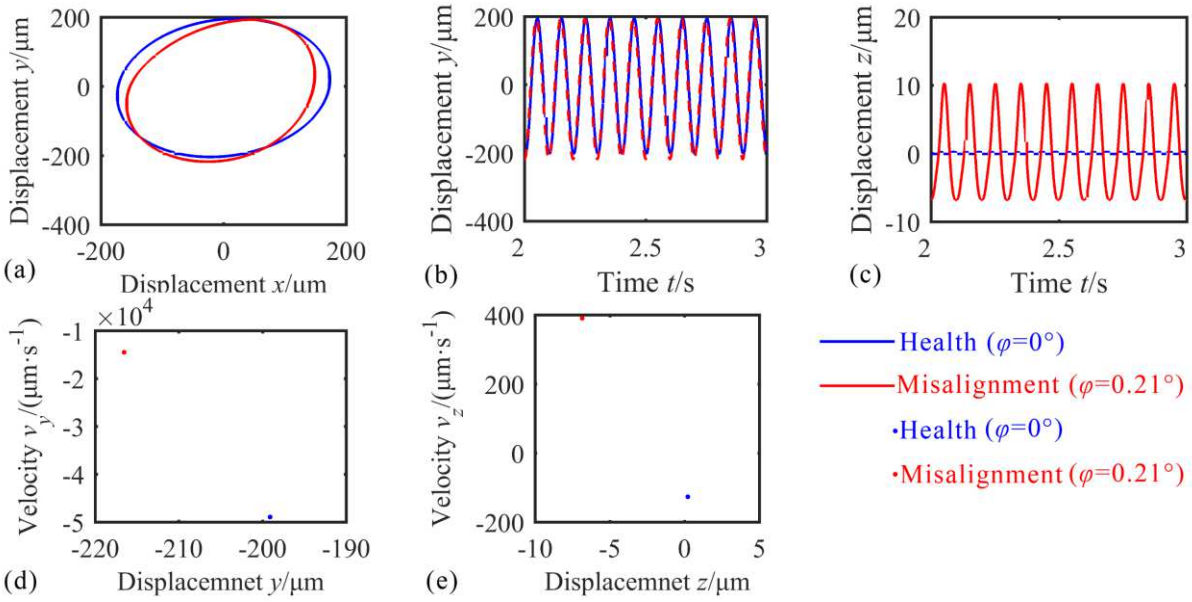

Fig. 18 System vibration response at n=11830r/min: (a) rotor orbit, (b) time-domain waveform in Y-direction, (c) time-domain waveform in Z-direction, (d) Poincaré section map in Y-direction and (e) Poincaré section map in Z-direction

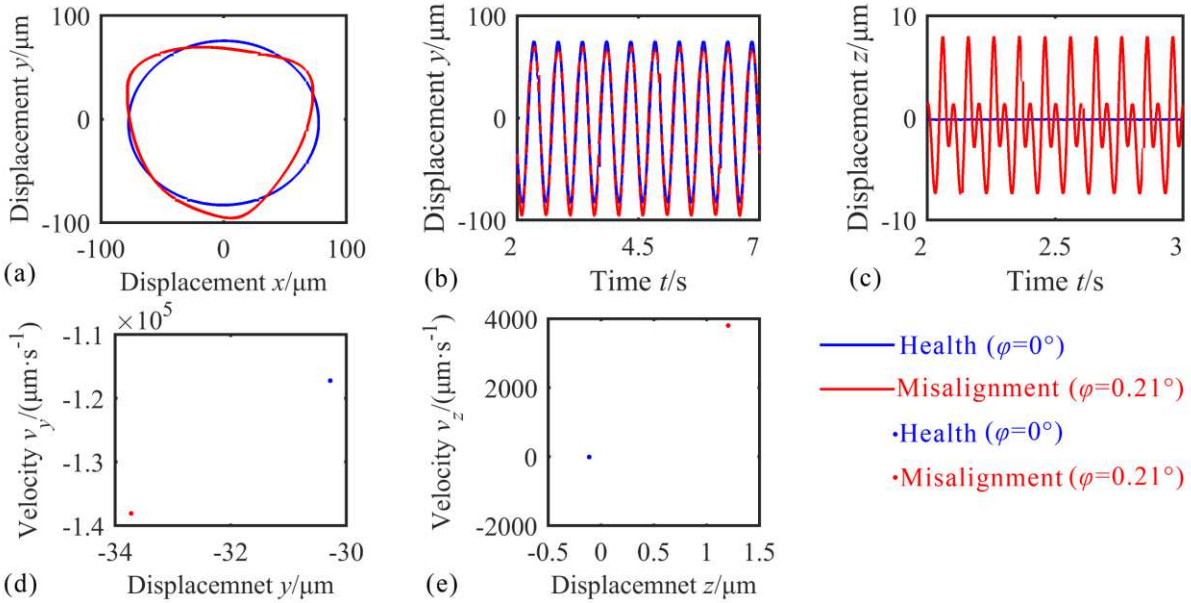

Fig. 19 System vibration response at n=15000r/min: (a) rotor orbit, (b) time-domain waveform in Y-direction, (c) time-domain waveform in Z-direction, (d) Poincaré section map in Y-direction and (e) Poincaré section map in Z-direction

4. Conclusions

In this paper, a dynamic model of the ball bearing-coupling-rotor system is established based on the finite element method. Based on the Hertz contact theory, a nonlinear force model of 5-DOF rolling bearing is proposed, which can consider the misalignment of bearing rings and the clearance of cage pockets. The coupling

misalignment excitation force model is further introduced. The radial and axial vibration responses of the system under the action of misalignment faults are analyzed. Some conclusions are as follows:

(1) When the rotor is running at low speed, the bearing misalignment greatly affects the dynamic characteristics of the rotor system, and the frequency component of bearing varying compliance vibration (f_{vc}) is obvious. Therefore, the influence of bearing misalignment cannot be ignored in the study of rotor misalignment. With the increase of operating speed, the VC vibration is relatively weakened, the rotor unbalance and coupling misalignment have a greater impact, and the component of $2f_r$ is more obvious. The reason is that the rotor unbalance force and coupling misalignment force are related to the square term of speed, while the bearing misalignment force is only related to the power of speed.

(2) Misalignment leads to periodic changes in the contact angle and radial clearance of each ball in the rolling bearing, and the velocity of each ball in the bearing is not equal. With the aggravation of misalignment, there may be two loading areas of the bearing. The contact force of the ball also increases, and the increase of the contact force can even reach 183.6%, which may lead to extrusion deformation between the ball and the raceway. In addition, the difference in ball rotational speed is more significant. The rotational speed of the ball and cage is inconsistent, which leads to the reciprocating extrusion and collision of the ball in the cage pocket, and increases the possibility of fatigue fracture of the cage.

(3) The bearing misalignment increases the support stiffness of the rotor, resulting in the enhancement of the critical speed of the system. The system vibration caused by bearing misalignment has strong directivity. In the subcritical speed range, the bearing misalignment reduces the amplitude of the radial vibration of the system, which is due to the increased constraint of the bearing on the rotor and the increased deflection of the rotor. The radial vibration of the system is aggravated by misalignment in critical and supercritical speed range.

(4) Due to the angular misalignment, the bearing produces a component of restoring force along the axial direction, so the axial vibration of the system increases under the action of this excitation. The more serious the misalignment, the greater the axial vibration of the rotor system. Therefore, axial vibration can be used as an essential basis to measure the angular misalignment fault of the deep groove ball bearing-rotor system.

Acknowledgements

The authors would like to acknowledge the support of the China North Vehicle Research Institute on the project (No. 2021JX02GC01).

Data availability

The datasets generated during and/or analyzed during the current study are available from the corresponding author on reasonable request.

Conflict of Interest

The authors declare that they have no conflict of interest.

References

[1] Rybczyński, J.: The possibility of evaluating turbo-set bearing misalignment defects on the basis of bearing trajectory features. Mechanical Systems and Signal Processing **25**, 521-536 (2011). https://doi.org/10.1016/j.ymssp.2010.07.011.

[2] Harris, T. A., Kotzalas, M.N.: Advanced concepts of bearing technology: Rolling bearing analysis. Taylor & Francis, Boca Raton (2006). https://doi.org/10.1201/9781420006582.

[3] ISO 15243: 2017, Rolling bearings-damage and failures-terms, characteristics and causes. International Organization for Standardization, Geneva, Switzerland (2017).

[4] Chen, C. H.: The common failures of aero-engine mechanical system. China Aviation Publishing & Media, Beijing (2013).(in Chinese)

[5] Gibbons, C. B.: Coupling misalignment forces. In: Proceedings of the 5th Turbomachinery Symposium, Texas A&M University, Gas Turbine Laboratories, pp.111-116 (1976). https://doi.org/10.21423/R10T1X

[6] Sekhar, A. S., Prabhu, B. S.: Effects of coupling misalignment on vibrations of rotating machinery. Journal of Sound and Vibration **185**, 655-671 (1995). https://doi.org/10.1006/jsvi.1995.0407

[7] Lee, Y. S., Lee, C. W.: Modelling and vibration analysis of misaligned rotor-ball bearing systems. Journal of Sound and Vibration **224**, 17-32 (1999). https://doi.org/10.1006/jsvi.1997.1301

[8] Zhao, G., Liu, Z. S., Chen, F.: Meshing force of misaligned spline coupling and the influence on rotor system. International Journal of Rotating Machinery **2008**, 321308 (2008). https://doi.org/10.1155/2008/321308

[9] Wu, K., Liu, Z. W., Ding, Q.: Vibration responses of rotating elastic coupling with dynamic spatial misalignment. Mechanism and Machine Theory **151**, 103916 (2020).https://doi.org/10.1016/j.mechmachtheory.2020.103916

[10] Liu, Y., Zhao, Y. L., Li, J. T., Lu, H. H., Ma, H.: Feature extraction method based on NOFRFs and its application in faulty rotor system with slight misalignment. Nonlinear Dyn **99**, 1763–1777 (2020). https://doi.org/10.1007/s11071-019-05340-8

[11] Al-Hussain, K. M., Redmond, I.: Dynamic response of two rotors connected by rigid mechanical coupling with parallel misalignment. Journal of Sound and Vibration **249**, 483-498 (2002). https://doi.org/10.1006/jsvi.2001.3866

[12] Al-Hussain, K. M.: Dynamic stability of two rigid rotors connected by a flexible coupling with angular misalignment. Journal of Sound and Vibration **266**, 217-234 (2003). https://doi.org/10.1016/S0022-460X(02)01627-9

[13] Lees, A. W.: Misalignment in rigidly coupled rotors. Journal of Sound and Vibration **305**, 261-271 (2007). https://doi.org/10.1016/j.jsv.2007.04.008

[14] Patel, T. H., Darpe, A. K.: Vibration response of misaligned rotors. Journal of Sound and Vibration **325**, 609-628 (2009). https://doi.org/10.1016/j.jsv.2009.03.024

[15] Sarkar, S., Nandi, A., Neogy, S., Dutt, J. K., Kundra, T. K.: Finite element analysis of misaligned rotors on oil-film bearings. Sadhana **35**, 45-61 (2010). https://doi.org/10.1007/s12046-010-0005-1

[16] da Silva Tuckmantel, F. W., Cavalca, K. L.: Vibration signatures of a rotor-coupling-bearing system under angular misalignment. Mechanism and Machine Theory **133**, 559-583 (2019). https://doi.org/10.1016/j.mechmachtheory.2018.12.014

[17] Srinivas, R. S., Tiwari, R., Babu, C. K.: Modeling, analysis, and identification of parallel and angular misalignments in a coupled rotor-bearing-active magnetic bearing system. Journal of Dynamic Systems, Measurement, and Control **143**, 011007 (2021). https://doi.org/10.1115/1.4048352

[18] Lal, M.: Modeling and estimation of speed dependent bearing and coupling misalignment faults in a turbine generator system. Mechanical Systems and Signal Processing **151**, 107365 (2021).https://doi.org/10.1016/j.ymssp.2020.107365

[19] Bouaziz, S., Messaoud, N. B., Mataar, M., Fakhfakh, T., Haddar, M.: A theoretical model for analyzing the dynamic behavior of a misaligned rotor with active magnetic bearings. Mechatronics **21**, 899-907 (2011). https://doi.org/10.1016/j.mechatronics.2011.05.001

[20] Patel, T. H., Darpe, A. K.: Experimental investigations on vibration response of misaligned rotors. Mechanical Systems and Signal Processing **23**, 2236-2252 (2009).https://doi.org/10.1016/j.ymssp.2009.04.004

[21] Lu, K., Jin, Y. L., Huang, P. F., Zhang, F., Zhang, H. P., Fu, C., Chen, Y. S.: The applications of POD method in dual rotor-bearing systems with coupling misalignment. Mechanical Systems and Signal Processing **150**, 107236 (2021). https://doi.org/10.1016/j.ymssp.2020.107236

[22] Jalan, A. K., Mohanty, A. R.: Model based fault diagnosis of a rotor–bearing system for misalignment and unbalance under steady-state condition. Journal of Sound and Vibration **327**, 604-622 (2009). https://doi.org/10.1016/j.jsv.2009.07.014

[23] Wang, N. F., Jiang, D. X.: Vibration response characteristics of a dual-rotor with unbalance-misalignment coupling faults: theoretical analysis and experimental study. Mechanism and Machine Theory **125**, 207-219 (2018). https://doi.org/10.1016/j.mechmachtheory.2018.03.009

[24] Desouki, M., Sassi, S., Renno, J., Gowid, S. A.: Dynamic response of a rotating assembly under the coupled effects of misalignment and imbalance. Shock and Vibration, 8819676 (2020). https://doi.org/10.1155/2020/8819676

[25] Fu, X. Q., Jia, W. T., Xu, H., Song, S. L.: Imbalance–misalignment–rubbing coupling faults in hydraulic turbine

vibration. Optik **127**, 3708-3712 (2016).https://doi.org/10.1016/j.ijleo.2016.01.006

[26] Jin, Y. L., Liu, Z. W., Yang, Y., Li, F. S., Chen, Y. S.: Nonlinear vibrations of a dual-rotor-bearing-coupling misalignment system with blade-casing rubbing. Journal of Sound and Vibration **497**, 115948 (2021). https://doi.org/10.1016/j.jsv.2021.115948

[27] Nataraj, M., Baskaran, G.: Experimental investigation of misalignment and looseness in rotor bearing system using Bartlett Power Spectral Density. Journal of Scientific & Industrial Research **76**, 308-313 (2017). http://nopr.niscair.res.in/handle/123456789/41597

[28] Ma, H., Wang, X. L., Niu, H. Q., Wen, B. C.: Oil-film instability simulation in an overhung rotor system with flexible coupling misalignment. Archive of Applied Mechanics **85**, 893-907 (2015). https://doi.org/10.1007/s00419-015-0998-3

[29] Li, Z. G., Jiang, J., Tian, Z.: Stochastic dynamics of a nonlinear misaligned rotor system subject to random fluid-induced forces. Journal of Computational and Nonlinear Dynamics **12**, 011004 (2017). https://doi.org/10.1115/1.4034124

[30] Hinton, W. R.: An investigation into the causes of ball bearing failures in types P2 and P3 engine-driven generators. Wear **16**, 3-42 (1970). https://doi.org/10.1016/0043-1648(70)90261-9.

[31] Crawford, T. S.: The experimental determination of ball bearing cage stress. Wear **16,** 43-52 (1970). https://doi.org/10.1016/0043-1648(70)90262-0.

[32] Xu, R., Shen, X. S., Fan, Q., Wang, X. Q., Chen, Y.: Failure analysis of aeroengine spindle ball bearing. Bearing, 20-24 (2012). https://doi.org/10.19533/j.issn1000-3762.2012.06.009. (in Chinese)

[33] Ertas, B. H., Vance, J. M.: The effect of static and dynamic misalignment on ball bearing radial stiffness. Journal of Propulsion and Power **20**, 634-647 (2004). https://doi.org/10.2514/1.11462.

[34] Liao, N. T., Lin, J. F.: An analysis of misaligned single-row angular-contact ball bearing. Journal of Mechanical Design **126**, 370-374 (2004). https://doi.org/10.1115/1.1667891

[35] Zhang, Y. F., Fang, B., Kong, L. F., Li, Y.: Effect of the ring misalignment on the service characteristics of ball bearing and rotor system. Mechanism and Machine Theory **151**, 103889 (2020). https://doi.org/10.1016/j.mechmachtheory.2020.103889

[36] Wen, C. W., Meng, X. H., Lyu, B. G., Gu, J. M., Xiao, L.: Influence of angular misalignment on the tribological performance of high-speed micro ball bearings considering full multibody interactions. Proceedings of the Institution of Mechanical Engineers, Part J: Journal of Engineering Tribology **235**, 1168-1189 (2021). https://doi.org/10.1177/1350650120948292

[37] Yang, Z. C., Zhang, Y., Zhang, K., Li, S. H.: Wear analysis of angular contact ball bearing in multiple-bearing spindle system subjected to uncertain initial angular misalignment. Journal of Tribology **143**, 091703 (2021). https://doi.org/10.1115/1.4049258

[38] Yang, L. H., Xu, T. F., Xu, H. L., Wu, Y.: Mechanical behavior of double-row tapered roller bearing under combined external loads and angular misalignment. International Journal of Mechanical Sciences **142-143**, 561-574 (2018).

https://doi.org/10.1016/j.ijmecsci.2018.04.056

[39] Zheng, J. Y., Ji, J. C., Yin, S., Tong, V. C.: Internal loads and contact pressure distributions on the main shaft bearing in a modern gearless wind turbine. Tribology International **141**, 105960 (2020). https://doi.org/10.1016/j.triboint.2019.105960

[40] Xu, T. F., Yang, L. H., Wu, W., Wang, K.: Effect of angular misalignment of inner ring on the contact characteristics and stiffness coefficients of duplex angular contact ball bearings. Mechanism and Machine Theory **157**, 104178 (2021). https://doi.org/10.1016/j.mechmachtheory.2020.104178

[41] Li, X. H., Lv, Y. F., Yan, K., Liu, J., Hong, J.: Study on the influence of thermal characteristics of rolling bearings and spindle resulted in condition of improper assembly. Applied Thermal Engineering **114**, 221-233 (2017). https://doi.org/10.1016/j.applthermaleng.2016.11.194

[42] Oktaviana, L., Tong, V. C., Hong, S. W.: Skidding analysis of angular contact ball bearing subjected to radial load and angular misalignment. Journal of Mechanical Science & Technology **33**, 837-845 (2019). https://doi.org/10.1007/s12206-019-0140-5

[43] Yi, J., Pang, B. T., Liu, H., Wang, F. T., Ji, B. W., Jing, M. Q.: Influence of misalignment on nonlinear dynamic characteristics for matched bearings-rotor system. Proceedings of the Institution of Mechanical Engineers Part K: Journal of Multi-body Dynamics **228**, 172-181 (2014). https://doi.org/10.1177/1464419313520143.

[44] Parmar, V., Saran, V. H., Harsha, S.: Effect of dynamic misalignment on the vibration response, trajectory followed and defect-depth achieved by the rolling-elements in a double-row spherical rolling-element bearing. Mechanism and Machine Theory **162**, 104366 (2021). https://doi.org/10.1016/j.mechmachtheory.2021.104366

[45] Yang, R., Jin, Y., Hou, L., Chen, Y. S.: Study for ball bearing outer race characteristic defect frequency based on nonlinear dynamics analysis. Nonlinear Dyn **90**, 781–796 (2017). https://doi.org/10.1007/s11071-017-3692-x

[46] Hou, L., Chen, Y. S., Cao, Q. J., Zhang, Z. Y.: Turning maneuver caused response in an aircraft rotor-ball bearing system. Nonlinear Dyn **79**, 229–240 (2015). https://doi.org/10.1007/s11071-014-1659-8

[47] Liew, H. V., Lim, T. C.: Analysis of time-varying rolling element bearing characteristics. Journal of Sound and Vibration **283**, 1163-1179 (2005). https://doi.org/10.1016/j.jsv.2004.06.022

[48] Petersen, D., Howard, C., Prime, Z.: Varying stiffness and load distributions in defective ball bearings: analytical formulation and application to defect size estimation. Journal of Sound and Vibration **337**, 284-300 (2015). https://doi.org/10.1016/j.jsv.2014.10.004

[49] Luo, Y. G., Wang, P. F., Jia, H. F., Huang, F. C.: Dynamic characteristics analysis of a seal-rotor system with rub-impact fault. Journal of Computational and Nonlinear Dynamics **16**, 081003 (2021). https://doi.org/10.1115/1.4051185.